AMERICAN SOCIETY FOR MICROBIOLOGY | Journal of Virology

Interferon-Regulatory Factor 5-Dependent Signaling Restricts Orthobunyavirus Dissemination to the Central Nervous System

Jose Luiz Proenca-Modena,[a,e] Jennifer L. Hyde,[a] Renata Sesti-Costa,[b,f] Tiffany Lucas,[a] Amelia K. Pinto,[a] Justin M. Richner,[a] Matthew J. Gorman,[b] Helen M. Lazear,[a,g] Michael S. Diamond[a,b,c,d]

Departments of Medicine,[a] Pathology & Immunology,[b] and Molecular Microbiology[c] and Center for Human Immunology and Immunotherapy Programs,[d] Washington University School of Medicine, St. Louis, Missouri, USA; Department of Genetics, Evolution and Bioagents, Institute of Biology, University of Campinas, Campinas, Brazil[e]; Department of Biochemistry and Immunology, University of São Paulo, Ribeirão Preto School of Medicine, Ribeirão Preto, Brazil[f]; Department of Microbiology and Immunology, University of North Carolina School of Medicine, Chapel Hill, North Carolina, USA[g]

ABSTRACT

Interferon (IFN)-regulatory factor 5 (IRF-5) is a transcription factor that induces inflammatory responses after engagement and signaling by pattern recognition receptors. To define the role of IRF-5 during bunyavirus infection, we evaluated Oropouche virus (OROV) and La Crosse virus (LACV) pathogenesis and immune responses in primary cells and in mice with gene deletions in *Irf3*, *Irf5*, and *Irf7* or in *Irf5* alone. Deletion of *Irf3*, *Irf5*, and *Irf7* together resulted in uncontrolled viral replication in the liver and spleen, hypercytokinemia, extensive liver injury, and an early-death phenotype. Remarkably, deletion of *Irf5* alone resulted in meningoencephalitis and death on a more protracted timeline, 1 to 2 weeks after initial OROV or LACV infection. The clinical signs in OROV-infected *Irf5*$^{-/-}$ mice were associated with abundant viral antigen and terminal deoxynucleotidyltransferase-mediated dUTP-biotin nick end labeling (TUNEL)-positive cells in several regions of the brain. Circulating dendritic cell (DC) subsets in *Irf5*$^{-/-}$ mice had higher levels of OROV RNA *in vivo* yet produced lower levels of type I IFN than wild-type (WT) cells. This result was supported by data obtained *in vitro*, since a deficiency of IRF-5 resulted in enhanced OROV infection and diminished type I IFN production in bone marrow-derived DCs. Collectively, these results indicate a key role for IRF-5 in modulating the host antiviral response in peripheral organs that controls bunyavirus neuroinvasion in mice.

IMPORTANCE

Oropouche virus (OROV) and La Crosse virus (LACV) are orthobunyaviruses that are transmitted by insects and cause meningitis and encephalitis in subsets of individuals in the Americas. Recently, we demonstrated that components of the type I interferon (IFN) induction pathway, particularly the regulatory transcription factors IRF-3 and IRF-7, have key protective roles during OROV infection. However, the lethality in *Irf3*$^{-/-}$ *Irf7*$^{-/-}$ (DKO) mice infected with OROV was not as rapid or complete as observed in *Ifnar*$^{-/-}$ mice, indicating that other transcriptional factors associated with an IFN response contribute to antiviral immunity against OROV. Here, we evaluated bunyavirus replication, tissue tropism, and cytokine production in primary cells and mice lacking IRF-5. We demonstrate an important role for IRF-5 in preventing neuroinvasion and the ensuing encephalitis caused by OROV and LACV.

The interferon (IFN)-regulatory factor (IRF) family of transcription factors has a central role in regulating innate immune cell development and responses (1). Several IRF family members (e.g., IRF-1, IRF-3, IRF-5, and IRF-7) are present in the cytoplasm in an inactive form and then phosphorylated after pattern recognition receptor engagement and signaling. These events facilitate nuclear translocation, binding to DNA promoter elements, and induction of antiviral and proinflammatory genes that modulate immunity (2). Canonical IFN induction pathways that are regulated by Toll-like receptors (TLRs) and RIG-I-like receptors (RLRs) converge on activation of IRF-3 and IRF-7 (3).

IRF-5 acts downstream of the TLR-MyD88 and RLR-MAVS signaling pathways, via a TRAF6- and IRAK1-dependent mechanism, to induce expression of proinflammatory cytokines, including interleukin-6 (IL-6), IL-12, and TNF-α (4). IRF-5 is expressed constitutively in several hematopoietic cells, including B cells, monocytes, macrophages (Mϕ), and dendritic cell (DC) subsets (5, 6). IRF-5 regulates differentiation of lymphoid cells and innate immune responses but also is implicated in oncogenesis and apoptosis (7, 8). During B cell development, IRF-5 regulates expression of Blimp-1, a protein required for the formation of immunoglobulin-secreting plasma cells. As a consequence, *Irf5*$^{-/-}$ mice have increased numbers of CD19^{+} B220^{-} cells and reduced plasma cell expansion and isotype switching in response to antigens or pathogens (9–11). A deficiency of IRF-5 also resulted in reduced IFN-α, IFN-β, and IL-6 production by TLR-7- and TLR-9-stimulated DCs or IL-6 production by B cells (9, 12), and this was associated with resistance to shock syndrome induced by unmethylated CpG DNA and lipopolysaccharide (LPS) (4). *Irf5* alleles with enhanced promoter activity are linked to autoimmune disorders in humans, including systemic lupus erythematosus,

Received 12 September 2015 **Accepted** 3 October 2015

Accepted manuscript posted online 14 October 2015

Citation Proenca-Modena JL, Hyde JL, Sesti-Costa R, Lucas T, Pinto AK, Richner JM, Gorman MJ, Lazear HM, Diamond MS. 2016. Interferon-regulatory factor 5-dependent signaling restricts orthobunyavirus dissemination to the central nervous system. J Virol 90:189–205. doi:10.1128/JVI.02276-15.

Editor: S. Perlman

Address correspondence to Michael S. Diamond, diamond@wusm.wustl.edu.

rheumatoid arthritis, Sjögren's syndrome, multiple sclerosis, and inflammatory bowel disease (13–16).

Recent studies have illustrated the importance of IRF-5 function in antiviral immunity (17). After MAVS signaling, IRF-5 acts coordinately with IRF-3 and IRF-7 to regulate type I IFN responses in myeloid DCs after West Nile virus (WNV) infection (18). In addition, IRF-5 shapes the early innate immune response against WNV in the draining lymph node (11). An IRF-5 deficiency was associated with lower levels of proinflammatory cytokines, chemokines, and activated immune cells in lymphoid tissues within 2 days of WNV infection (11). *Irf5*$^{-/-}$ mice also had a mildly blunted WNV-specific antibody response, with fewer antigen-specific memory B cells and long-lived plasma cells (11).

Oropouche virus (OROV) is an arthropod-transmitted, enveloped, negative-sense orthobunyavirus of the family *Bunyaviridae* that has caused periodic outbreaks of a debilitating febrile illness in South America (19). Oropouche fever is the second most frequent arthropod-transmitted viral disease in Brazil, and more than 500,000 cases have been confirmed in Brazil, Peru, Trinidad, Panama, and Suriname (19–21). OROV infection can progress to meningitis and/or encephalitis in some patients (22–24). Despite its clinical importance, little is known about the factors that determine OROV dissemination into the central nervous system (CNS).

A recent study in mice with targeted gene deletions provided insight into mechanisms of innate immune restriction of OROV infection (25). The host type I IFN antiviral response is essential for controlling OROV infection, as mice lacking IFN-α/β receptor (*Ifnar*$^{-/-}$) or signaling molecules and transcription factors involved in IFN production (e.g., *Mavs*$^{-/-}$, *Irf3*$^{-/-}$, or *Irf7*$^{-/-}$) sustained high levels of virus replication in the liver and spleen (25). However, *Irf3*$^{-/-}$ *Irf7*$^{-/-}$ double-knockout (DKO) mice were not as vulnerable to OROV or La Crosse virus (LACV) (a second orthobunyavirus) infection as were *Ifnar*$^{-/-}$ mice (25), suggesting that additional transcriptional factors regulated IFN-dependent antiviral immunity.

To define the role of IRF-5 in restricting OROV infection, we infected *Irf5*$^{-/-}$, *Irf3*$^{-/-}$ *Irf7*$^{-/-}$ DKO, or *Irf3*$^{-/-}$ *Irf5*$^{-/-}$ *Irf7*$^{-/-}$ triple-knockout (TKO) mice with OROV. Whereas the combined loss of *Irf3* and *Irf7* or *Irf3*, *Irf5*, and *Irf7* expression resulted in rapid systemic disease with high lethality rates and extensive virus replication in the liver, the deletion of *Irf5* alone yielded a distinct phenotype. OROV infection in *Irf5*$^{-/-}$ mice was associated with a protracted disease that recapitulated features of human infection, with signs of neurological involvement and high levels of virus accumulating in the brain and spinal cord.

MATERIALS AND METHODS

Ethics statement. This study was carried out in accordance with the recommendations in the *Guide for the Care and Use of Laboratory Animals* of the National Institutes of Health. The protocols were approved by the Institutional Animal Care and Use Committee at the Washington University School of Medicine (Assurance no. A3381-01). Inoculations were performed under anesthesia that was induced and maintained with ketamine hydrochloride and xylazine, and all efforts were made to minimize animal suffering.

Viruses. OROV (strain BeAn 19991) and LACV (original strain) were provided by E. Arruda (São Paulo University, Ribeirão Preto, Brazil) and A. Pekosz (Johns Hopkins University, Baltimore, MD, USA), respectively. OROV and LACV stocks were produced in Vero cells. Studies with OROV were conducted under enhanced biosafety level 3 (BSL3) and animal BSL3 (A-BSL3) containment at Washington University School of Medicine with appropriate personal protective equipment (respirators) and approval from the U.S. Department of Agriculture. Experiments with LACV were performed under BSL2 and A-BSL2 conditions.

Mouse experiments. Wild-type (WT) C57BL/6 mice were purchased from Jackson Laboratories. Congenic *Ifnar*$^{-/-}$, *Irf5*$^{-/-}$, *Irf3*$^{-/-}$ *Irf7*$^{-/-}$ DKO, and *Irf3*$^{-/-}$ *Irf5*$^{-/-}$ *Irf7*$^{-/-}$ TKO mice have been described previously (4, 18, 26, 27). *Irf5*$^{-/-}$ mice were the gift of T. Taniguchi (Tokyo, Japan), obtained from I. Rifkin (Boston, MA), and had been backcrossed for eight generations. After detection of a homozygous *Dock2* mutation in this line, we backcrossed *Irf5*$^{-/-}$ mice for five additional generations and selected animals that were *Dock2*$^{wt/wt}$ using PCR-based genotyping (11). All mice were bred in a specific-pathogen-free facility at Washington University. Subcutaneous inoculations were performed by injection in the footpad with 10^6 focus-forming units (FFU) of OROV and 10^5 FFU of LACV in a volume of 50 μl. Intracranial injections were performed with 10^2 FFU of OROV in a volume of 10 μl. Infection experiments were designed with 5- to 6-week-old mice and 8-week-old mice for OROV and LACV, respectively. The 8-week-old mice were used with LACV because younger WT mice had a higher mortality rate, which limited our ability to detect differences in the KO mice. Survival and weight loss were monitored for 21 days.

Measurement of viral burden. OROV-infected mice were euthanized at days 4, 6, 9, and 12 postinfection. LACV-infected mice were euthanized at days 4, 8, and 12 postinfection. Animals were perfused extensively with 20 ml of phosphate-buffered saline (PBS) at the time of euthanasia. Liver, spleen, kidney, lung, heart, brain, and spinal cord were harvested, weighed, and homogenized with zirconia beads in MagNA Lyser instrument (Roche Life Science) in 1 ml of minimal essential medium (MEM) supplemented with 2% heat-inactivated fetal bovine serum (FBS). All homogenized tissues and approximately 200 μl of serum from infected animals were stored at −80°C until virus titration.

Viral burden was determined by focus-forming assay on Vero cells. Samples were thawed, clarified by centrifugation (2,000 × *g* at 4°C for 10 min), and then diluted serially prior to infection of Vero cells in 96-well plates. Infected-cell foci were detected 22 to 24 h later, following overnight fixation with 1% paraformaldehyde and incubation with a 1:1,000 dilution of polyclonal mouse anti-OROV ascites fluid (ATCC, VR1228AF) or a 1:100 dilution of hybridoma cell supernatants containing the anti-LACV monoclonal antibodies (MAbs) 807-31 and 807-33 (provided by A. Pekosz), all in a volume of 50 μl for 2 h at room temperature. After incubation for 1 h with 50 μl of a 1:2,000 dilution of horseradish peroxidase (HRP)-conjugated goat anti-mouse IgG (Sigma), foci were detected by addition of TrueBlue detection reagent (KPL). The spots were analyzed with a CTL Immunospot instrument.

Measurement of viral RNA. Tissue samples from WT and *Irf5*$^{-/-}$ mice were extracted with the RNeasy kit (Qiagen). OROV RNA levels in serum, liver, spleen, lung, kidney, brain, and spinal cord were determined by TaqMan one-step quantitative reverse transcriptase PCR (qRT-PCR) and expressed on a $\log_{10}$ scale as viral RNA equivalents per gram or per milliliter after comparison with a standard curve produced using serial 10-fold dilutions of OROV RNA. The amplification of the glyceraldehyde-3-phosphate dehydrogenase (GAPDH) gene (IdT catalog no. Mm.PT.39a.1) was used as a control for normalization. All reactions were performed using 300 ng of RNA, 2.5 μl of 10× PrimeTime solution (IdT) (OROV-F, 5′-TACCCAGATGCGATCACCAA-3′; OROV-R, 5′-TTGCG TCACCATCATTCCAA-3′; OROV-Probe, 5′-/56-FAM/TGCCTTTGGC TGAGGTAAAGGGCTG/36-TAMSp/-3′), 12.5 μl of TaqMan master mix (Applied Biosystems), and 0.625 μl of reverse transcriptase (Applied Biosystems) in a final volume of 25 μl. The cycling algorithm was 48°C for 30 min, 95°C for 10 min, and 45 cycles of 95°C for 15 s and 60°C for 1 min.

Blood chemistry analysis. Serum from WT, *Irf5*$^{-/-}$, or TKO mice was isolated on days 4, 6, 9, and 12 after OROV infection. Chemistry analyses were performed using a Catalyst Dx Chemistry Analyzer (IDEX Laboratories) after treatment with β-propiolactone (BPL) (Sigma) for 30 min at 37°C to inactivate infectious virus. Treatment with BPL did not impact chemistry results.

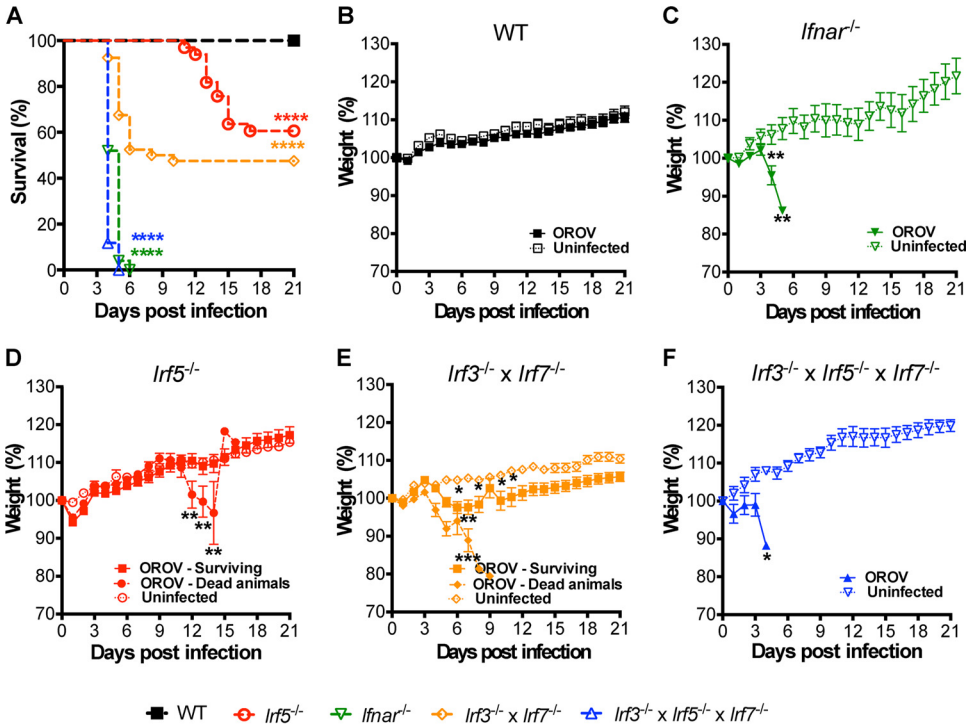

FIG 1 *Irf3*$^{-/-}$ *Irf5*$^{-/-}$ *Irf7*$^{-/-}$ TKO mice are vulnerable to OROV infection, whereas deletion of IRF-5 alone induces a disease with a protracted course. (A) Survival analysis of 6-week-old mice after inoculation with 10^6 PFU of OROV by subcutaneous inoculation in the footpad. WT ($n = 33$), *Ifnar*$^{-/-}$ ($n = 25$), *Irf5*$^{-/-}$ ($n = 33$), *Irf3*$^{-/-}$ *Irf7*$^{-/-}$ DKO ($n = 39$), and *Irf3*$^{-/-}$ *Irf5*$^{-/-}$ *Irf7*$^{-/-}$ TKO ($n = 17$) mice were used. Data are pooled from at least three independent experiments. Asterisks indicate differences that were statistically significant with a comparison to WT mice by the log rank test (****, $P < 0.0001$). (B to F) Weight loss of infected (dead or surviving animals considered separately) and noninfected WT ($n = 33$ and $n = 10$ for infected and noninfected mice, respectively) (B), *Ifnar*$^{-/-}$ ($n = 25$ infected and $n = 3$ noninfected) (C), *Irf5*$^{-/-}$ ($n = 20$ dead, $n = 13$ survivors, and $n = 4$ noninfected) (D), *Irf3*$^{-/-}$ *Irf7*$^{-/-}$ DKO ($n = 19$ dead, $n = 20$ survivors, and $n = 13$ noninfected) (E), and *Irf3*$^{-/-}$ *Irf5*$^{-/-}$ *Irf7*$^{-/-}$ TKO ($n = 17$ infected, $n = 3$ noninfected) (F) mice. The weight loss curves were compared using 2-way ANOVA. Asterisks indicate differences that were statistically significant with a comparison to noninfected mice (*, $P < 0.05$; **, $P < 0.01$; ***, $P < 0.001$).

Cytokine bioplex assay. At days 4, 6, 9, and 12 after OROV infection of WT, *Irf5*$^{-/-}$, and TKO mice, serum was collected and cytokine levels were measured using the Bioplex Pro mouse cytokine assay (Bio-Rad). The levels of the following cytokines and chemokines were determined: IL-1α, IL-1β, IL-2, IL-3, IL-4, IL-6, IL-9, IL-10, IL-12p40, IL-12p70, IL-13, IL-17, eotaxin (CCL11), granulocyte colony-stimulating factor (G-CSF), granulocyte-macrophage colony-stimulating factor (GM-CSF), IFN-γ, KC (CXCL1), monocyte chemoattractant protein 1 (MCP-1) (CCL-2), MIP-1α (CCL3), MIP-1β (CCL4), RANTES (CCL5), and TNF-α.

Quantification of type I IFN activity. Levels of type I IFN in the sera of WT and *Irf5*$^{-/-}$ mice at 1, 2, or 3 days after OROV were determined by an encephalomyocarditis virus cytopathic effect bioassay in L929 cells as described previously (28). Briefly, all samples were treated with citrate buffer (40 mM citric acid, 10 mM KCl, 135 mM NaCl [pH 3.0]) for 10 min and neutralized with minimal essential medium buffered with 45 mM HEPES, pH 8.0. The amount of type I IFN per milliliter of serum was calculated and compared to a standard curve using recombinant IFN-α (PBL Assay Science).

Histology, TUNEL staining, and immunohistochemistry. Liver and spleen tissues were obtained from WT, *Irf5*$^{-/-}$, and TKO mice at day 4 after OROV infection. Brain tissue from WT and *Irf5*$^{-/-}$ KO mice was harvested at day 12 after virus inoculation. All samples were fixed in 4% paraformaldehyde (in PBS) for 24 h at 4°C, dehydrated in increasing ethanol concentrations, and embedded in paraffin. Hematoxylin-eosin staining of paraffin-embedded tissues was performed by the Digestive Diseases Research Core Center Morphology Core of Washington University. Terminal deoxynucleotidyltransferase-mediated dUTP-biotin nick end labeling (TUNEL) staining from liver and spleen sections was performed using an *in situ* cell death detection kit, peroxidase (POD) (Roche), as described by the manufacturer. TUNEL staining of brain sections was performed after permeabilization with proteinase K (Roche) for 30 min using the cell death detection kit, tetramethylrhodamine (TMR) red (Roche), followed by counterstaining with DAPI (4′,6′-diamidino-2-phenylindole) (Invitrogen) for 5 min. As a positive control, tissue sections were treated with DNase (Sigma) for 10 min to introduce nicks into DNA. Slides were visualized using an Axioskop (Zeiss) microscope, and images were captured using AxioCam HRm (Zeiss) and AxioVision Rel4.8 (Zeiss) software.

For OROV antigen detection, tissues sections were deparaffinized, rehydrated, and treated with citrate buffer (pH 6.0) for antigen retrieval. Endogenous peroxidases were quenched by incubation with 4% H_2O_2 for 30 min, and the antigen detection was performed using the "Mouse on Mouse" (MOM) immunodetection kit according to the manufacturer's protocol (Vector Laboratories). All sections were incubated with an avidin-biotin blocking solution and MOM mouse immunoglobulin-blocking reagent for 15 min at room temperature and then incubated with mouse polyclonal anti-OROV ascites fluid (1:100) for 2 h at room temperature. Sections were then incubated with a MOM biotinylated anti-mouse IgG antibody for 1 h and with a streptavidin-peroxidase Ultrasensitive Polimer (Sigma) for 15 min at room temperature. Antigen-positive cells were visualized at magnifications of ×20 and ×40 in a Zeiss Axioskop microscope, and images were captured using an AxioCam MRC digital color camera after incubation with 3,3′-diaminobenzidine (DAB)-HRP substrate (Vector) and counterstaining with hematoxylin.

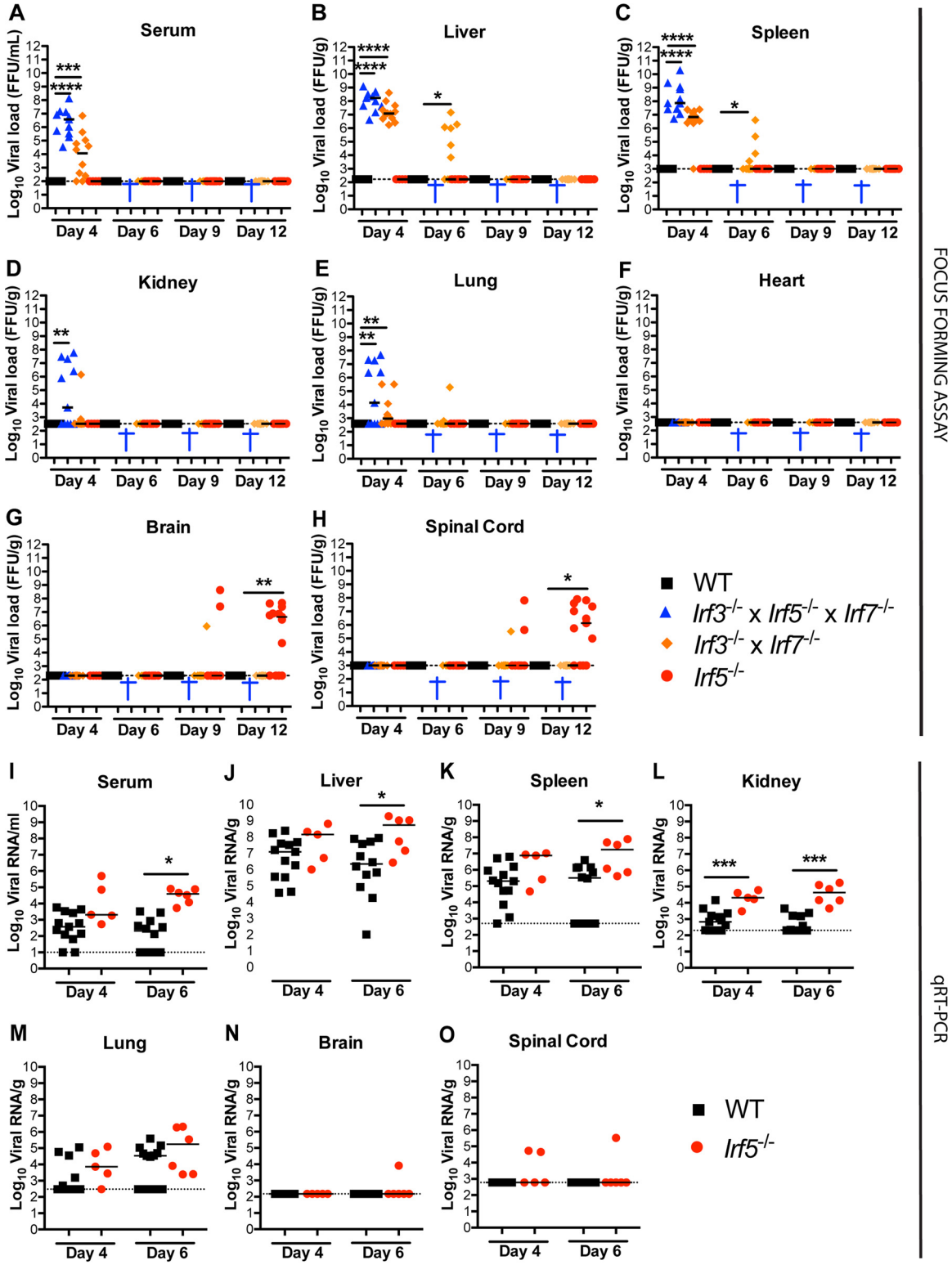

FIG 2 Viral burden in mice infected with OROV. (A to H) Viral burden after OROV infection of WT, *Irf5*$^{-/-}$, *Irf3*$^{-/-}$ *Irf7*$^{-/-}$ DKO, and *Irf3*$^{-/-}$ *Irf5*$^{-/-}$ *Irf7*$^{-/-}$ TKO mice was measured by focus-forming assay in samples from serum (A), liver (B), spleen (C), kidney (D), lung (E), heart (F), brain (G), and spinal cord (H). (I to O) Viral burden after OROV infection of WT and *Irf5*$^{-/-}$ mice was determined by qRT-PCR in samples from serum (I), liver (J), spleen (K), kidney (L), lung (M), brain (N), and spinal cord (O). Data points represent individual mice. Bars indicate median values and were obtained from 6 to 15 mice per time point. Dashed lines represent the limit of sensitivity of the assay. Asterisks indicate statistical significance as judged by the Mann-Whitney test with a comparison to WT mice (*, $P < 0.05$; **, $P < 0.01$; ***, $P < 0.001$; ****, $P < 0.0001$). A blue cross indicates that all OROV-infected TKO animals were dead at the indicated time point. The viral burden data from *Irf3*$^{-/-}$ *Irf7*$^{-/-}$ DKO mice at days 4 and 6 after OROV infection were published previously (25) and are provided as a comparison to the *Irf3*$^{-/-}$ *Irf5*$^{-/-}$ *Irf7*$^{-/-}$ TKO mice.

TABLE 1 Blood urea nitrogen, alkaline phosphatase, and creatine kinase levels after OROV infection[a]

Test	Genotype	4 dpi		6 dpi		9 dpi		12 dpi	
		Value	*P*	Value	*P*	Value	*P*	Value	*P*
BUN[b]	WT	22.5 ± 3.02		22.0 ± 3.4		19.0 ± 2.42		19.5 ± 3.88	
	Irf5$^{-/-}$	19.5 ± 7.27	0.10	14.0 ± 3.5	0.07	17.0 ± 3.3	0.34	21.5 ± 6.8	0.99
	TKO	19.0 ± 5.5	0.25	Dead		Dead		Dead	
ALKP[c]	WT	144 ± 34.6		161 ± 41.0		177 ± 10.9		126 ± 30.3	
	Irf5$^{-/-}$	125 ± 31.3	0.26	134 ± 25.7	0.27	123 ± 21.6	0.09	151 ± 64.4	0.71
	TKO	103 ± 56.8	0.14	Dead		Dead		Dead	
CK[d]	WT	5066 ± 1761		6657 ± 888		379.5 ± 171		551 ± 161	
	Irf5$^{-/-}$	6215 ± 585	0.46	6666 ± 999	0.26	3088 ± 820	0.05	3133 ± 998	0.05
	TKO	6478 ± 1315	0.92	Dead		Dead		Dead	

[a] WT, *Irf5*$^{-/-}$ or *Irf3*$^{-/-}$ *Irf5*$^{-/-}$ *Irf7*$^{-/-}$ (TKO) mice were inoculated with OROV. Serum was collected at 4, 6, 9, and 12 days postinfection (dpi), and blood chemistry was measured by a Catalyst Dx Chemistry Analyzer. Data represent the mean ± standard deviation for 5 to 11 mice per group. Statistical significance was determined using the Mann-Whitney test, and *P* values were obtained after comparison to WT mice infected in parallel.
[b] BUN was quantified in mg/dl.
[c] ALKP was quantified in U/liter.
[d] CK was quantified in U/liter.

OROV replication in primary cells. Macrophage (Mϕ) and DC cultures were derived from bone marrow isolated from WT, *Irf5*$^{-/-}$, and TKO mice and cultured for 7 days in medium supplemented with 40 ng/ml M-CSF (PeproTech) or 20 ng/ml of both GM-CSF and IL-4 (PeproTech), respectively. Multistep virus growth curves were determined using a multiplicity of infection (MOI) of 0.001. The viral titer in the cell-free supernatant was determined by FFU assay on Vero cells at the following time points after infection: 0, 1, 4, 12, 24, 36, 48, and 60 h.

Isolation of OROV-infected cells. Whole blood was collected in tubes containing EDTA. Erythrocytes were removed after 10 min of incubation in red blood cell lysis solution buffer (Miltenyi Biotech). Nonspecific antibody binding was inhibited after incubation with Fc block (BD Bioscience) for 15 min. Cell suspensions from six different WT and *Irf5*$^{-/-}$ mice were purified sequentially by positive selection with CD19, CD3, and CD11b microbeads (Miltenyi Biotech), following the manufacturer's protocol. A separate experiment was conducted to purify plasmacytoid DC (pDCs) using B220 or CD11c microbeads (Miltenyi Biotech). All cell populations were tested by qRT-PCR for OROV and *Gapdh* RNA levels and analyzed in parallel by flow cytometry by staining with antibodies to CD3, CD19, CD11b, and CD11c.

Quantification of *Ifna* and *Ifnb* RNAs. The levels of *Ifna* and *Ifnb* mRNAs were determined by qRT-PCR in DCs, Mϕ, and sorted cells from WT and *Irf5*$^{-/-}$ mice, following previously published procedures (25). Briefly, RNA from target cells was extracted using the RNeasy kit (Qiagen) and treated with Turbo DNase (Life Technologies) for 2 h at 37°C. qRT-PCR was performed by one-step reaction with previously described primers and probes (25). All reactions were assembled in a final volume of 25 μl with 300 ng of RNA, 1× PrimeTime mix (Integrated DNA Technologies), and 12.5 μl of TaqMan master mix (Applied Biosystems) by using the cycling algorithm described above. All reactions were normalized to *Gapdh* RNA using previously published primers and probe (25), and results were expressed on a $\log_2$ scale as fold increase over mock according to the threshold cycle ($\Delta\Delta C_T$) method (29).

Quantitation of antibodies. The titer of neutralizing antibodies was determined on serum obtained at days 8 and 12 after OROV infection of WT and *Irf5*$^{-/-}$ mice by a standard plaque reduction neutralization assay (30). Plaques were scored visually after incubation with serial dilutions of the mice serum, and the 50% plaque reduction neutralization titer ($PRNT_{50}$) was determined.

Data analysis. All data were analyzed with Prism software (GraphPad Software). Kaplan-Meier survival curves were analyzed by the log rank test, and weight losses were compared using 2-way analysis of variance (ANOVA). For viral burden analysis, the log titers were analyzed by the Mann-Whitney test. qRT-PCR results also were compared using 2-way ANOVA. A *P* value of <0.05 indicated statistically significant differences.

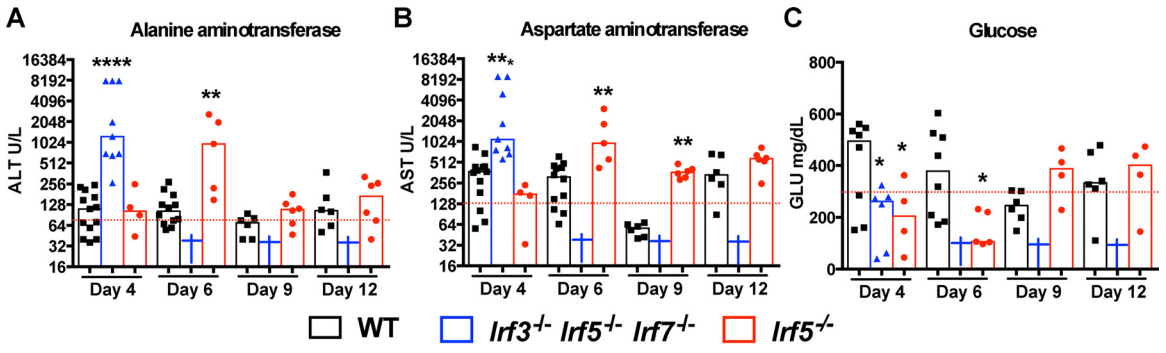

FIG 3 Blood chemistry reveals liver injury after OROV infection in *Irf5*$^{-/-}$ and *Irf3*$^{-/-}$ *Irf5*$^{-/-}$ *Irf7*$^{-/-}$ TKO mice. Alanine aminotransferase (ALT) (A), aspartate aminotransferase (AST) (B), and glucose (GLU) (C) levels were measured from serum samples of WT, *Irf5*$^{-/-}$ and *Irf3*$^{-/-}$ *Irf5*$^{-/-}$ *Irf7*$^{-/-}$ TKO mice ($n = 4$ to 13 for each group) obtained 4, 6, 9, and 12 days after infection with 10^6 FFU of OROV. Data points represent individual mice and were pooled from two independent experiments. Asterisks indicate statistical significance with a comparison to WT mice as judged by the Mann-Whitney test (*, $P < 0.05$; **, $P < 0.01$; ***, $P < 0.001$; ****, $P < 0.0001$). Dashed lines represent the mean values obtained from three mock-infected animals.

TABLE 2 Serum cytokine and chemokine levels after OROV infection[a]

Cytokine	Genotype	4 dpi		6 dpi		9 dpi		12 dpi	
		pg/ml	*P*	pg/ml	*P*	pg/ml	*P*	pg/ml	*P*
IL-1α	WT	1.0 ± 1.58		3.6 ± 2.3		1.2 ± 2.1		0.8 ± 1.8	
	Irf5$^{-/-}$	2.5 ± 4.3	056	2.5 ± 7.9	0.84	3.4 ± 4.1	0.69	2.1 ± 5.1	0.51
	TKO	0.0 ± 12.8	0.57	Dead		Dead		Dead	
IL-1β	WT	199 ± 44		200 ± 53		192 ± 24		180 ± 18	
	Irf5$^{-/-}$	260 ± 156	0.22	145 ± 294	0.71	188 ± 74	0.89	225 ± 123	0.64
	TKO	175 ± 138	0.53	Dead		Dead		Dead	
IL-2	WT	18.3 ± 14.6		17.5 ± 21.9		16.7 ± 11.4		17.8 ± 9.0	
	Irf5$^{-/-}$	50.1 ± 39.1	0.32	43.1 ± 77.3	0.26	22.8 ± 11.5	0.78	11.5 ± 11.2	0.41
	TKO	7.0 ± 19.3	0.02	Dead		Dead		Dead	
IL-3	WT	7.5 ± 11.9		16.4 ± 13.2		21.5 ± 6.1		26.1 ± 8.9	
	Irf5$^{-/-}$	7.8 ± 4.3	0.50	6.9 ± 7.1	0.29	39.9 ± 21.8	0.38	36.2 ± 19.2	0.52
	TKO	6.9 ± 19.2	0.82	Dead		Dead		Dead	
IL-4	WT	0.0 ± 8.3		7.5 ± 9.0		14.2 ± 5.8		15.9 ± 6.5	
	Irf5$^{-/-}$	0.0 ± 4.8	0.42	0.0 ± 2.6	0.17	24.0 ± 12.6	0.29	22.7 ± 11.3	0.45
	TKO	0.0 ± 1.3	0.41	Dead		Dead		Dead	
IL-5	WT	15.0 ± 7.5		17.4 ± 7.1		22.9 ± 5.1		21.6 ± 4.9	
	Irf5$^{-/-}$	20.0 ± 10.0	0.75	19.2 ± 19.8	0.76	25.3 ± 13.1	0.41	11.3 ± 10.5	0.62
	TKO	8.7 ± 4.3	0.06	Dead		Dead		Dead	
IL-6	WT	4.5 ± 1.5		5.0 ± 2.9		4.2 ± 0.9		4.7 ± 1.3	
	Irf5$^{-/-}$	8.9 ± 6.0	0.17	4.5 ± 7.8	0.55	6.9 ± 2.9	0.07	6.1 ± 3.9	0.9
	TKO	100 ± 301	<0.0001	Dead		Dead		Dead	
IL-9	WT	117 ± 115		68 ± 131		0.0 ± 7.9		0.0 ± 16.9	
	Irf5$^{-/-}$	213 ± 237	0.35	0.0 ± 143	0.49	0.0 ± 0.0	0.99	0.0 ± 0.0	0.99
	TKO	0.0 ± 96	0.24	Dead		Dead		Dead	
IL-10	WT	20.8 ± 16.3		24.5 ± 14.4		20.1 ± 11.7		21.7 ± 7.0	
	Irf5$^{-/-}$	53.5 ± 27.7	0.17	57.0 ± 44.6	0.30	34.3 ± 17.6	0.78	28.1 ± 16.9	0.9
	TKO	10.0 ± 27.9	0.58	Dead		Dead		Dead	
IL-12 (p40)	WT	29.3 ± 30.9		29.8 ± 17.6		19.5 ± 1.5		22.2 ± 7.5	
	Irf5$^{-/-}$	27.8 ± 5.9	0.51	32.0 ± 16.5	0.71	31.0 ± 11.5	0.06	22.6 ± 10.0	0.87
	TKO	191 ± 125	<0.0001	Dead		Dead		Dead	
IL-12 (p70)	WT	23.9 ± 12.2		24.8 ± 8.8		22.8 ± 2.2		23.6 ± 4.3	
	Irf5$^{-/-}$	33.8 ± 17.9	0.23	26.8 ± 25.6	0.85	53.6 ± 28.5	0.38	49.5 ± 27.5	0.64
	TKO	22.6 ± 13.9	0.98	Dead		Dead		Dead	
IL-13	WT	28.8 ± 26.2		45.8 ± 52.1		26.5 ± 38.2		35.4 ± 11.5	
	Irf5$^{-/-}$	89.8 ± 281.4	0.054	216 ± 330	0.19	25.2 ± 23.8	0.66	11.5 ± 26.4	0.62
	TKO	13.4 ± 62.0	0.30	Dead		Dead		Dead	
IL-17	WT	5.6 ± 5.1		8.7 ± 6.6		12.8 ± 3.2		13.2 ± 4.1	
	Irf5$^{-/-}$	7.6 ± 4.0	0.87	5.8 ± 5.4	0.53	23.1 ± 14.8	0.37	20.4 ± 11.8	0.64
	TKO	7.5 ± 5.3	0.91	Dead		Dead		Dead	
Eotaxin	WT	455 ± 287		502 ± 230		513 ± 135		454 ± 221	
	Irf5$^{-/-}$	527 ± 413	0.87	512 ± 796	0.94	559 ± 517	0.89	281 ± 490	0.62
	TKO	30.9 ± 221	0.02	Dead		Dead		Dead	
G-CSF	WT	15.9 ± 5.2		14.8 ± 5.5		15.0 ± 1.8		18.1 ± 4.2	
	Irf5$^{-/-}$	15.9 ± 30.0	0.94	9.6 ± 13.6	0.47	29.9 ± 22.5	0.38	19.3 ± 14.0	0.77
	TKO	1499 ± 2899	<0.0001	Dead		Dead		Dead	

(Continued on following page)

TABLE 2 (Continued)

Cytokine	Genotype	4 dpi		6 dpi		9 dpi		12 dpi	
		pg/ml	*P*	pg/ml	*P*	pg/ml	*P*	pg/ml	*P*
GM-CSF	WT	64.4 ± 26.6		75.9 ± 29.3		94.9 ± 15.7		93.8 ± 24.0	
	Irf5$^{-/-}$	60.6 ± 37.9	0.47	35.5 ± 61.3	0.34	109.9 ± 66.4	0.77	106.8 ± 62	0.64
	TKO	39.8 ± 30.3	0.16	Dead		Dead		Dead	
IFN-γ	WT	2.1 ± 2.1		2.4 ± 1.4		1.9 ± 0.5		1.6 ± 0.7	
	Irf5$^{-/-}$	4.7 ± 2.7	0.34	3.4 ± 7.5	0.76	2.1 ± 0.8	0.29	1.6 ± 1.8	0.9
	TKO	2.1 ± 3.1	0.97	Dead		Dead		Dead	
KC	WT	30.0 ± 9.6		31.1 ± 19.7		23.0 ± 2.8		27.3 ± 7.8	
	Irf5$^{-/-}$	24.4 ± 42	0.87	24.3 ± 14.5	0.24	37.7 ± 20.8	0.07	19.8 ± 9.3	0.87
	TKO	151 ± 465	<0.0001	Dead		Dead		Dead	
MCP-1	WT	226 ± 113		237 ± 132		252 ± 59		222 ± 61	
	Irf5$^{-/-}$	252 ± 141	0.42	279 ± 235	0.59	300 ± 219	0.99	134 ± 230	0.62
	TKO	146 ± 273	0.92	Dead		Dead		Dead	
MIP-1α	WT	1.8 ± 1.4		2.2 ± 1.8		2.6 ± 1.3		2.8 ± 1.4	
	Irf5$^{-/-}$	0.5 ± 0.7	0.18	2.4 ± 6.4	0.84	4.7 ± 2.6	0.3	3.2 ± 2.2	0.92
	TKO	13.1 ± 9.7	0.0016	Dead		Dead		Dead	
MIP-1β	WT	38.5 ± 22.4		47.7 ± 20.4		53.1 ± 6.6		55.0 ± 10.0	
	Irf5$^{-/-}$	34.0 ± 20.1	0.51	44.6 ± 29.7	0.79	71.0 ± 40.2	0.36	76.9 ± 38.7	0.62
	TKO	14.4 ± 10.6	0.02	Dead		Dead		Dead	
RANTES	WT	15.1 ± 5.8		14.9 ± 5.1		14.5 ± 1.2		16.1 ± 2.3	
	Irf5$^{-/-}$	16.7 ± 1.7	0.27	16.6 ± 18.2	0.76	29.7 ± 16.0	0.38	25.8 ± 14.3	0.64
	TKO	20.3 ± 15.1	0.01	Dead		Dead		Dead	
TNF-α	WT	271 ± 193		370 ± 182		425 ± 65		451 ± 111	
	Irf5$^{-/-}$	358 ± 198	0.97	230 ± 307	0.47	621 ± 354	0.38	596 ± 347	0.64
	TKO	130 ± 302	0.36	Dead		Dead		Dead	

[a] WT, *Irf5*$^{-/-}$ or *Irf3*$^{-/-}$ *Irf5*$^{-/-}$ *Irf7*$^{-/-}$ (TKO) mice were inoculated with OROV. Serum was collected at 4, 6, 9, and 12 days postinfection, and cytokines and chemokines were measured by Bio-Plex array. Data represent the mean ± standard deviation for 5 to 11 mice per group. Statistical significance was determined using the Mann-Whitney test, and *P* values were obtained after comparison to WT mice infected in parallel.

RESULTS

***Irf3*$^{-/-}$ *Irf5*$^{-/-}$ *Irf7*$^{-/-}$ TKO mice are highly vulnerable to OROV infection.** Because the lethality in *Irf3*$^{-/-}$ *Irf7*$^{-/-}$ DKO mice after OROV infection was not as rapid or complete as that observed in *Ifnar*$^{-/-}$ mice (25) (Fig. 1A, C, and E), we hypothesized that other transcription factors implicated in the induction of antiviral immunity restricted OROV pathogenesis. Accordingly, we evaluated OROV pathogenesis in 5- to 6-week-old *Irf3*$^{-/-}$ *Irf5*$^{-/-}$ *Irf7*$^{-/-}$ TKO mice after injection with 10^6 FFU of OROV by a subcutaneous route. Analogous to results with *Ifnar*$^{-/-}$ mice, OROV infection of TKO mice caused rapid weight loss and resulted in 100% mortality, with a mean of survival time of 4 days (Fig. 1A, C, and F). OROV-infected *Irf3*$^{-/-}$ *Irf5*$^{-/-}$ *Irf7*$^{-/-}$ TKO mice exhibited lethargy and decreased body temperature, especially at day 4 after infection, but did not show signs of neuroinvasive disease, such as ataxia, seizures, tremors, or paralysis.

Vulnerability of *Irf5*$^{-/-}$ mice to OROV infection. To assess the role of IRF-5 in restricting OROV infection more directly, we inoculated 5- to 6-week-old *Irf5*$^{-/-}$ and congenic wild-type (WT) mice with OROV. Whereas 39% of *Irf5*$^{-/-}$ mice succumbed to OROV infection, WT mice had no mortality or signs of morbidity (Fig. 1A and B). *Irf5*$^{-/-}$ mice exhibited a protracted course of OROV disease compared to *Irf3*$^{-/-}$ *Irf5*$^{-/-}$ *Irf7*$^{-/-}$ TKO mice, with signs of neurological involvement and lethality starting at days 7 and 9 after infection, respectively (Fig. 1A, D, and F). Almost 50% of *Irf5*$^{-/-}$ OROV-infected mice developed signs of severe disease after day 7, including lethargy, shivering, ataxia, limb paralysis, dyskinesia, hypothermia, and weight loss.

Viral burden studies. To determine the basis for their susceptibility to OROV infection, we inoculated WT, *Irf5*$^{-/-}$, *Irf3*$^{-/-}$ *Irf7*$^{-/-}$ DKO, and *Irf3*$^{-/-}$ *Irf5*$^{-/-}$ *Irf7*$^{-/-}$ TKO mice and measured viral burdens in the serum, liver, spleen, kidney, lung, heart, brain, and spinal cord at days 4, 6, 9, and 12 after infection. As reported previously, infectious OROV was not recovered from any site in WT mice at any of the days analyzed (25). In comparison, all *Irf3*$^{-/-}$ *Irf5*$^{-/-}$ *Irf7*$^{-/-}$ TKO mice developed viremia (3.4×10^3 to 1.3×10^8 FFU/ml), and infectious OROV was recovered from the liver (4.2×10^6 to 1.3×10^9 FFU/g) and spleen (5.2×10^6 to 1.9×10^{10} FFU/g) at day 4 after infection (Fig. 2A to C). Infectious OROV also was present in the kidneys (5.2×10^3 to 5.9×10^7 FFU/g) and lungs (1.3×10^3 to 4.8×10^7 FFU/g) of approximately 50% of *Irf3*$^{-/-}$ *Irf5*$^{-/-}$ *Irf7*$^{-/-}$ TKO mice on day 4 (Fig. 2D and E). However, OROV was not recovered from heart, brain, or spinal cord of *Irf3*$^{-/-}$ *Irf5*$^{-/-}$ *Irf7*$^{-/-}$ TKO mice at this time point (Fig. 2F to H). The levels of OROV in the sera, livers, and spleens of

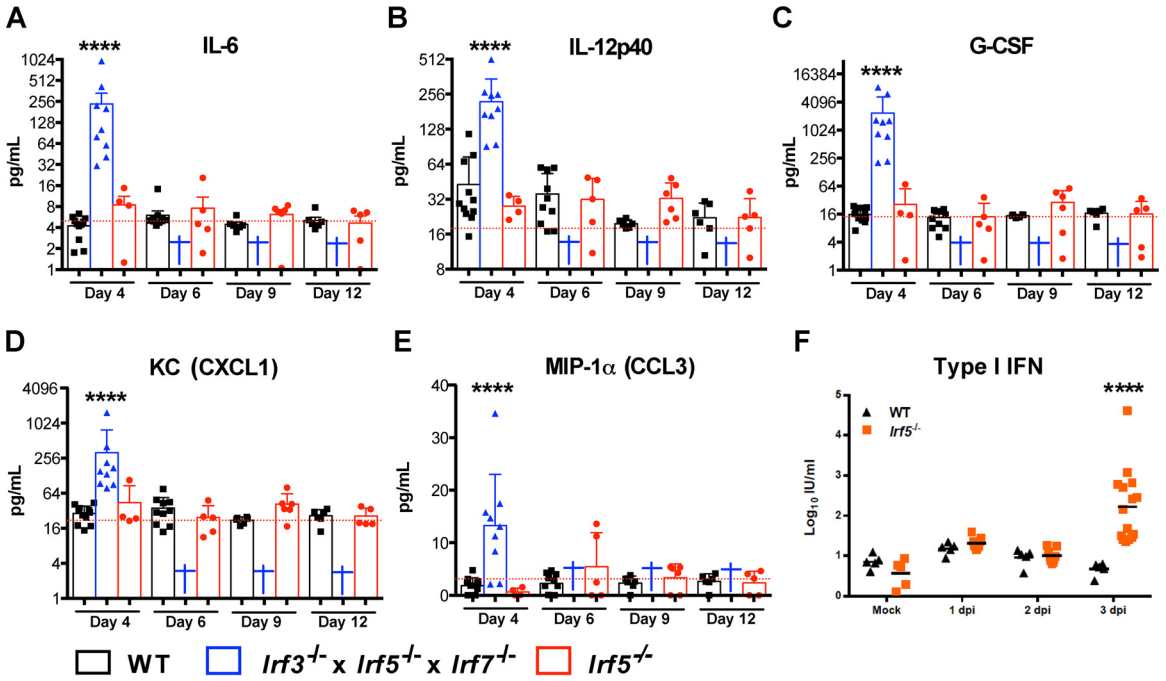

FIG 4 Serum cytokine levels in OROV-infected *Irf5*$^{-/-}$ and *Irf3*$^{-/-}$ *Irf5*$^{-/-}$ *Irf7*$^{-/-}$ TKO mice. (A to E) WT, *Irf5*$^{-/-}$, and *Irf3*$^{-/-}$ *Irf5*$^{-/-}$ *Irf7*$^{-/-}$ TKO mice were infected with 10^6 FFU of OROV. Four, 6, 9, or 12 days later, serum was collected and the levels of the indicated cytokines were determined. Data points represent individual mice, and the bars indicate the mean values ± standard deviations (SD). A blue cross indicates that all OROV-infected *Irf3*$^{-/-}$ *Irf5*$^{-/-}$ *Irf7*$^{-/-}$ TKO animals were dead at the indicated time point. The data correspond to 4 to 13 mice per each group from two independent experiments. Asterisks indicate statistical significance compared to serum from OROV-infected WT mice as judged by the Mann-Whitney test (***, $P < 0.001$; ****, $P < 0.0001$). Dashed lines represent the mean values from three mock-infected animals. (F) WT and *Irf5*$^{-/-}$ mice were infected with OROV, and 1, 2, and 3 days later, the type I IFN activity in serum was measured by an EMCV inhibition bioassay. Data are shown as the means for 5 to 10 mice per group from two independent experiments, and asterisks represent statistical significance as determined by 2-way ANOVA (****, $P < 0.0001$).

Irf3$^{-/-}$ *Irf5*$^{-/-}$ *Irf7*$^{-/-}$ TKO mice were similar to those reported for *Ifnar*$^{-/-}$ mice (*post hoc* comparison with *Ifnar*$^{-/-}$ mice [25], $P = 0.38$, 0.16, and 0.14, respectively) but greater those observed in *Irf3*$^{-/-}$ *Irf7*$^{-/-}$ DKO mice ($P = 0.005$, 0.013, and 0.003, respectively).

In contrast to the case for *Irf3*$^{-/-}$ *Irf5*$^{-/-}$ *Irf7*$^{-/-}$ TKO mice, infectious OROV was detected only in the brain and spinal cord at 9 days or after in *Irf5*$^{-/-}$ mice (Fig. 2G and H) and was not detected in any of the peripheral organs. At day 12, 9 of 13 (69%) *Irf5*$^{-/-}$ mice had measurable OROV in the brain or spinal cord, with high titers recovered (5.1×10^4 to 4.8×10^7 FFU/g and 5×10^5 to 8×10^7 FFU/g, respectively). In comparison, only 1 of 11 *Irf3*$^{-/-}$ *Irf7*$^{-/-}$ DKO mice had measurable infectious OROV in the brain and spinal cord at days 9 after inoculation, and no virus was measured at day 12 (Fig. 2G and H). These results suggest that IRF-5, rather than IRF-3 or IRF-7, preferentially regulates a stage of OROV control which is essential for restricting dissemination to or infection within the CNS.

To evaluate further whether IRF-5 limits OROV earlier in the course of infection, we evaluated the viral burden levels by a more sensitive quantitative reverse transcriptase PCR (qRT-PCR) assay. At day 6 after infection, higher levels of OROV RNA were observed in the sera (188-fold, $P = 0.0001$), livers (248-fold, $P = 0.02$), spleens (55-fold, $P = 0.03$), and kidneys (204-fold, $P = 0.0001$) of *Irf5*$^{-/-}$ mice than in those of WT mice (Fig. 2I to O).

Blood chemistry analysis reveals transient liver damage in OROV-infected *Irf5*$^{-/-}$ mice. Our prior study showed that deficiencies of type I IFN signaling (*Ifnar*$^{-/-}$), RIG-I-like receptor signaling (*Mavs*$^{-/-}$), or downstream transcription factors (*Irf3*$^{-/-}$ and *Irf7*$^{-/-}$) resulted in uncontrolled replication of OROV in peripheral organs that was associated with extensive liver damage (25). To assess whether visceral organ damage occurred in *Irf5*$^{-/-}$ mice after OROV infection, we measured the levels of alanine aminotransferase (ALT), aspartate aminotransferase (AST), glucose (GLU), blood urea nitrogen (BUN), creatinine (CRE), alkaline phosphatase (ALKP), and creatine kinase (CK) in the sera of WT, *Irf5*$^{-/-}$, and *Irf3*$^{-/-}$ *Irf5*$^{-/-}$ *Irf7*$^{-/-}$ TKO mice. Although BUN, ALKP, and CK levels were similar in infected WT and KO animals (Table 1), higher levels of ALT (1,243 U/liter and 969 U/liter) and AST (1,097 U/liter and 965U/liter) and lower levels of GLU (262 mg/dl and 106 mg/dl) were detected in the sera of *Irf3*$^{-/-}$ *Irf5*$^{-/-}$ *Irf7*$^{-/-}$ TKO and *Irf5*$^{-/-}$ mice at days 4 and 6 after OROV infection, respectively, than in WT animals (Fig. 3A to C). In contrast to that observed in *Irf3*$^{-/-}$ *Irf5*$^{-/-}$ *Irf7*$^{-/-}$ TKO and *Ifnar*$^{-/-}$ mice (25), the lethality observed in *Irf5*$^{-/-}$ mice was not associated with massive hepatic injury, since the levels of ALT, AST, and GLU normalized at later time points, even in the subset of animals that became ill.

Analysis of serum cytokine levels in *Irf5*$^{-/-}$ mice infected with OROV. IRF-5 has been reported to regulate serum cytokine accumulation in the context of arthropod-borne virus infections *in vivo* (11). We measured the levels of 23 cytokines and chemokines in sera from WT, *Irf5*$^{-/-}$, and *Irf3*$^{-/-}$ *Irf5*$^{-/-}$ *Irf7*$^{-/-}$ TKO mice on days 4, 6, 9, and 12 after OROV infection. Similar to published data (25) for *Ifnar*$^{-/-}$ *and Irf3*$^{-/-}$ *Irf7*$^{-/-}$ DKO mice, we did not observe elevated levels of vasoactive (e.g., TNF-α) or

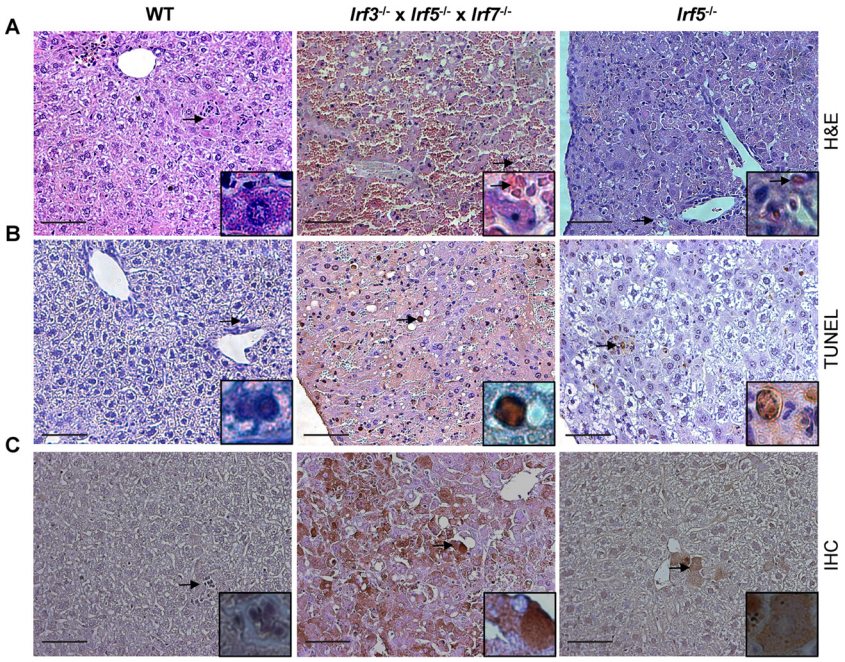

FIG 5 Analysis of liver tissue from OROV-infected WT, *Irf5*$^{-/-}$, and *Irf3*$^{-/-}$ *Irf5*$^{-/-}$ *Irf7*$^{-/-}$ TKO mice. (A) Histological (hematoxylin and eosin staining) analysis of the livers of infected mice harvested 4 days after OROV infection. (B) Representative images of TUNEL staining of livers of infected mice taken 4 days after OROV infection. (C) Detection of OROV antigen in livers of infected mice 4 days after virus infection. Images (magnification, ×20) were obtained from one representative animal from groups of three. Inset images show a higher magnification image (×40) and correspond to the region marked by the arrow. Scale bar = 100 μm.

inflammasome-generated (e.g., IL-1β) cytokines in the OROV-infected *Irf3*$^{-/-}$ *Irf5*$^{-/-}$ *Irf7*$^{-/-}$ TKO or *Irf5*$^{-/-}$ mice (Table 2). However, the levels of other proinflammatory cytokines and chemokines (e.g., IL-6, IL-12p40, G-CSF, KC, and MIP-1α) were increased at day 4 after OROV infection in *Irf3*$^{-/-}$ *Irf5*$^{-/-}$ *Irf7*$^{-/-}$ TKO mice (Fig. 4A to E). Because the levels of all analyzed cytokines were similar in *Irf5*$^{-/-}$ and WT mice after OROV infection, the mild liver damage observed in *Irf5*$^{-/-}$ mice is unlikely to be due to a generalized cytokine storm.

To assess whether a deficiency of IRF-5 affected systemic type I IFN responses, we measured type I IFN antiviral activity in sera from WT and *Irf5*$^{-/-}$ animals at days 1, 2, and 3 after OROV infection using an established bioassay (28). At day 1 after OROV infection, *Irf5*$^{-/-}$ and WT mice both had slightly higher levels of type I IFN than mock-infected mice (Fig. 4F). Type I IFN activity in serum waned in WT animals after 2 days of infection. However, significant increases in type I IFN were apparent (~44-fold, $P < 0.0001$) at day 3 after OROV injection in *Irf5*$^{-/-}$ mice. These high levels of type I IFN in *Irf5*$^{-/-}$ mice suggest an ongoing OROV infection and a relatively intact systemic IFN response.

OROV-induced disease in *Irf3*$^{-/-}$ *Irf5*$^{-/-}$ *Irf7*$^{-/-}$ TKO mice is associated with viral replication and hepatocyte death. To characterize the basis of the liver injury observed in *Irf3*$^{-/-}$ *Irf5*$^{-/-}$ *Irf7*$^{-/-}$ TKO infected mice, we performed pathological analysis on hepatic tissue isolated from WT, *Irf5*$^{-/-}$, and *Irf3*$^{-/-}$ *Irf5*$^{-/-}$ *Irf7*$^{-/-}$ TKO mice at day 4 after OROV infection. While hematoxylin-and-eosin staining revealed areas of edema and focal cellular necrosis in liver sections of *Irf3*$^{-/-}$ *Irf5*$^{-/-}$ *Irf7*$^{-/-}$ TKO mice, these changes were not apparent in samples from WT and *Irf5*$^{-/-}$ infected mice (Fig. 5A). The liver damage in *Irf3*$^{-/-}$ *Irf5*$^{-/-}$ *Irf7*$^{-/-}$ TKO mice was associated with greater numbers of terminal deoxynucleotidyltransferase-mediated dUTP-biotin nick end labeling (TUNEL)-positive (Fig. 5B) and OROV antigen-positive (Fig. 5C) hepatocytes at day 4 after infection. In comparison, a smaller number of TUNEL- and OROV-positive cells were observed in the livers of *Irf5*$^{-/-}$ mice, and none were detected in WT mice.

Effect of IRF-5 on OROV-induced neuropathology. Given the presence of OROV in the brain and spinal cord of some *Irf5*$^{-/-}$ mice (Fig. 2), we performed histological analysis on brain sections from WT and *Irf5*$^{-/-}$ mice to define why some animals succumbed to infection. TUNEL-positive cells were detected in different regions of the brain, including the cerebral cortex, hippocampus, midbrain, and cerebellum, from OROV-infected *Irf5*$^{-/-}$ mice (Fig. 6A to D). Moreover, abundant staining for viral antigen was detected in several regions of the brain of OROV-infected *Irf5*$^{-/-}$ mice but not in infected WT or uninfected *Irf5*$^{-/-}$ mice (Fig. 7A to D). In agreement with a published study that reported costaining for viral antigen with a neuron marker (NeuN) in newborn mice infected with OROV (31), the morphology of viral antigen-positive cells in *Irf5*$^{-/-}$ mice was consistent with neurons being targeted for infection (Fig. 7B and C), particularly in the hippocampus.

WT and *Irf5*$^{-/-}$ mice are equally vulnerable to OROV infection when inoculated by an intracranial route. To define whether the enhanced replication of OROV in the brains of *Irf5*$^{-/-}$ mice was due to an intrinsic inhibitory effect of IRF-5 in the CNS, we infected WT and *Irf5*$^{-/-}$ mice with OROV by an intracranial route and monitored morbidity, mortality, and viral burden. We observed no differences in survival rates, weight loss, and viral load in the brains of WT and *Irf5*$^{-/-}$ mice after intracranial infection (data not shown); 100% of WT and *Irf5*$^{-/-}$ mice succumbed to

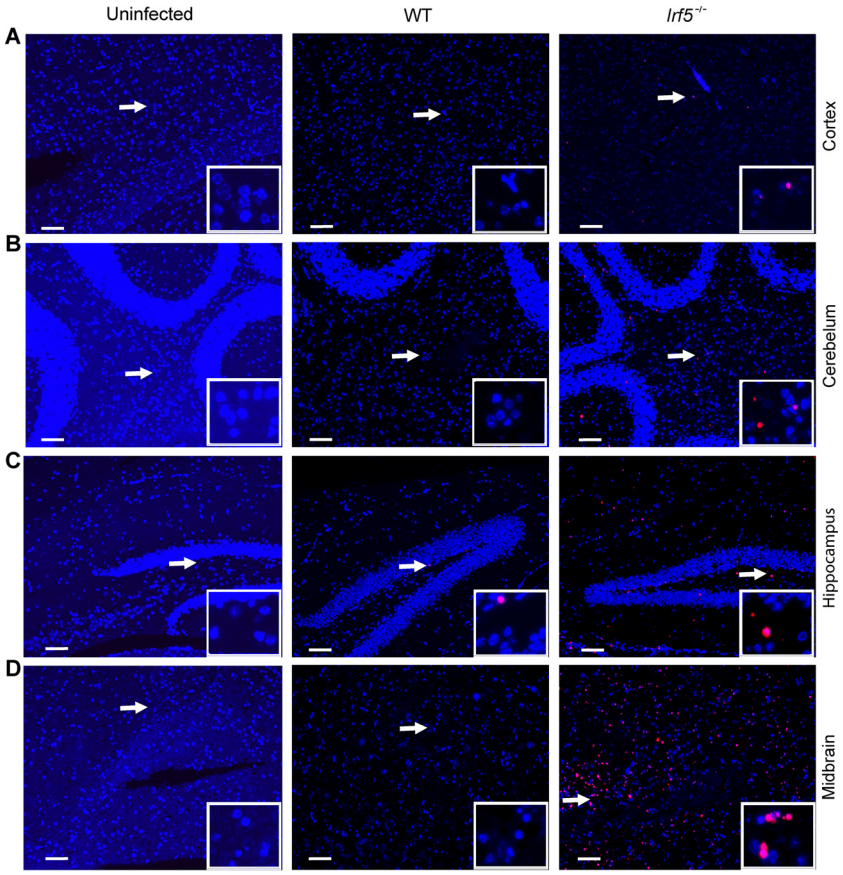

FIG 6 Dying cells are present in the brains of OROV-infected *Irf5*$^{-/-}$ mice. TUNEL analysis of the cerebral cortex (A), cerebellum (B), hippocampus (C), and midbrain (D) from mice harvested 12 days after OROV infection is shown. Representative images (magnification, ×10) were obtained from three mice of each group. Inset images show a magnified image and correspond to the region marked by the arrow. Scale bars = 100 μm.

infection by day 7 after intracranial inoculation, with no difference in mean time to death (data not shown). These results suggest that IRF-5 does not have a direct antiviral effect against OROV within the brain but rather is likely important for restricting spread to the brain.

OROV RNA persists in cells from *Irf5*$^{-/-}$ mice. To begin to define why a deficiency of IRF-5 resulted in disseminated OROV infection in the CNS at such a relatively late time point, we tested tissue samples for virus by qRT-PCR at days 9 and 12 after infection, which immediately precedes the onset of lethality in *Irf5*$^{-/-}$ mice (Fig. 1). Although samples from all WT mice tested were negative for OROV RNA at day 12, indicating successful clearance, the sera, livers, spleens, kidneys, lungs, brains, and spinal cords from more than 50% of *Irf5*$^{-/-}$ mice were positive for OROV RNA at this late time point (Fig. 8A to G). Analogously, at day 9 after infection, 3 of 8 (37.5%) and 5 of 8 (62.5%) spinal cord and brain samples, respectively, from *Irf5*$^{-/-}$ mice were positive for OROV RNA, whereas none were positive in infected WT mice (Fig. 8F and G). The persistence of OROV in different peripheral organs in *Irf5*$^{-/-}$ mice could lead to the selection of an encephalitic variant of OROV with greater neuroinvasive potential, as seen with the JC polyomavirus (32, 33). To test this idea, we homogenized brain tissue from OROV-infected *Irf5*$^{-/-}$ mice and used this to infect WT and *Irf5*$^{-/-}$ mice. These isolates were not more virulent or neuroinvasive than the parental OROV used in this study in either WT or *Irf5*$^{-/-}$ mice (data not shown).

As an alternative hypothesis, we speculated that persistently infected *Irf5*$^{-/-}$ cells might deliver OROV into the CNS. To determine which cells in *Irf5*$^{-/-}$ mice harbored OROV RNA during late stages of this disease, WT and *Irf5*$^{-/-}$ mice were infected with OROV. As we did not have a fluorescence-activated cell sorter in our enhanced BSL3 suite, at day 8 after viral infection, different cell populations were purified from blood by positive selection with anti-CD19, -CD3, -CD11b, -B220, or -CD11c magnetic beads (Fig. 9A and B) and tested by qRT-PCR for the presence of OROV RNA. Populations of CD11c^{+} and B220^{+} cells from *Irf5*$^{-/-}$ mice were frequently (~50%) positive for OROV (Fig. 9C), suggesting that these cells might transport virus into the brain directly or propagate virus sufficiently to allow crossing of the blood-brain barrier (BBB) in the fluid phase.

To evaluate whether a deficiency of IRF-5 could affect the expression of type I IFN in DCs *in vivo*, we measured the levels of *Ifnb* mRNA in CD11c^{+}, B220^{+}, CD11c^{-}, and B220^{-} cell populations from WT and *Irf5*$^{-/-}$ mice obtained 8 days after OROV infection. The levels of *Ifnb* mRNA were lower in circulating cells (including CD11c^{+} cells [18-fold, $P < 0.05$] and B220^{+} cells [23-fold, $P < 0.05$]) from *Irf5*$^{-/-}$ infected mice than in those from WT mice (Fig. 9D) despite the increased levels of OROV infection. These data suggest that IRF-5 signaling is essential to induce optimal type I IFN responses in peripheral blood mononuclear cells (PBMCs) after OROV infection.

OROV replication is enhanced and the production of type I

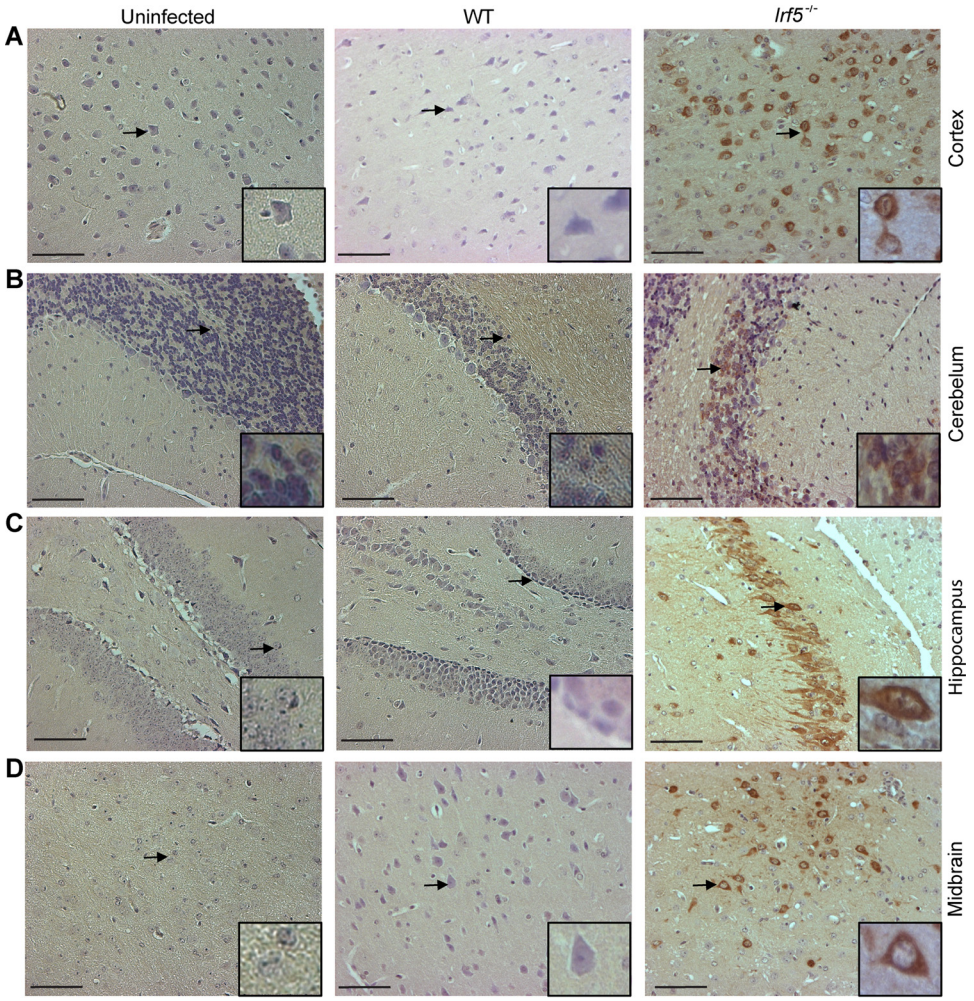

FIG 7 OROV detection in the brains of *Irf5*$^{-/-}$ mice after 12 days of infection. Immunohistochemical analysis after staining with polyclonal anti-OROV ascites fluid of the cerebral cortex (A), cerebellum (B), hippocampus (C) and midbrain (D) from uninfected, WT, and *Irf5*$^{-/-}$ infected mice. Images are derived from one representative animal obtained from a group of three animals. All sections were taken at 12 days of infection and the images were obtained using a magnification of ×20. A higher resolution of infected cells is shown in the inset with a higher magnification image (40×), corresponding to the region marked by the arrow. Scale bars = 100 μm.

IFN is diminished in DCs from *Irf5*$^{-/-}$ mice. As DCs from *Irf5*$^{-/-}$ mice produced less *Ifnb* and appeared to support greater OROV replication in blood, to corroborate these findings, we evaluated viral growth kinetics and type I IFN mRNA expression in bone marrow-derived DCs and Mϕ from WT, *Irf5*$^{-/-}$, and *Irf3*$^{-/-}$ *Irf5*$^{-/-}$ *Irf7*$^{-/-}$ TKO mice. In DCs, OROV infection was greater in cells derived from *Irf3*$^{-/-}$ *Irf5*$^{-/-}$ *Irf7*$^{-/-}$ TKO cells (>10,000-fold [$P < 0.01$]) at 36 to 60 h than in WT cells, which failed to support productive infection (Fig. 10A). Higher levels (130- to 1,750-fold higher, $P < 0.05$) of viral replication also were observed in DCs from *Irf5*$^{-/-}$ mice than in those from WT mice. In comparison, in Mϕ, productive OROV infection was detected only in cells derived from *Irf3*$^{-/-}$ *Irf5*$^{-/-}$ *Irf7*$^{-/-}$ TKO and not WT or *Irf5*$^{-/-}$ mice (Fig. 10B). Thus, in cell culture a deficiency of IRF5 resulted in enhanced OROV infection specifically in DCs, which supports our *ex vivo* and *in vivo* findings of elevated OROV RNA in *Irf5*$^{-/-}$ CD11c^{+} cells and sustained viremia and spread to the CNS in *Irf5*$^{-/-}$ mice. Moreover, and despite the higher levels of OROV infection, lower levels of *Ifna* and *Ifnb* mRNA were observed in bone marrow-derived DCs from *Irf5*$^{-/-}$ mice than in those from WT mice (Fig. 10C and D). A lesser impact of IRF-5 on *Ifna* but not *Ifnb* mRNA induction was observed in bone marrow-derived Mϕ after OROV infection (Fig. 10E and F).

Effect of IRF-5 on antibody responses after OROV infection. WT mice efficiently cleared OROV infection from all tissue compartments, whereas infection persisted in mice lacking IRF-5. Given prior studies demonstrating skewed antibody isotype responses, deficient B cell maturation, and low levels of antigen-specific memory B cells in *Irf5*$^{-/-}$ mice (9, 11, 34), we hypothesized that IRF-5 might be required for optimal adaptive immunity against OROV. To evaluate the role of IRF-5 in the humoral response against OROV, we determined the titers of neutralizing antibody at days 8 and 12 after infection in WT and *Irf5*$^{-/-}$ mice (Fig. 11A and B). *Irf5*$^{-/-}$ mice had only slightly lower neutralizing titers at days 8 (2.1-fold, $P < 0.005$) and 12 (1.5-fold, $P < 0.01$) than WT mice. To assess the importance of IRF-5 in the B cell response against OROV, we generated bone marrow chimeric mice that differed only in the expression of IRF-5 in B cells. We

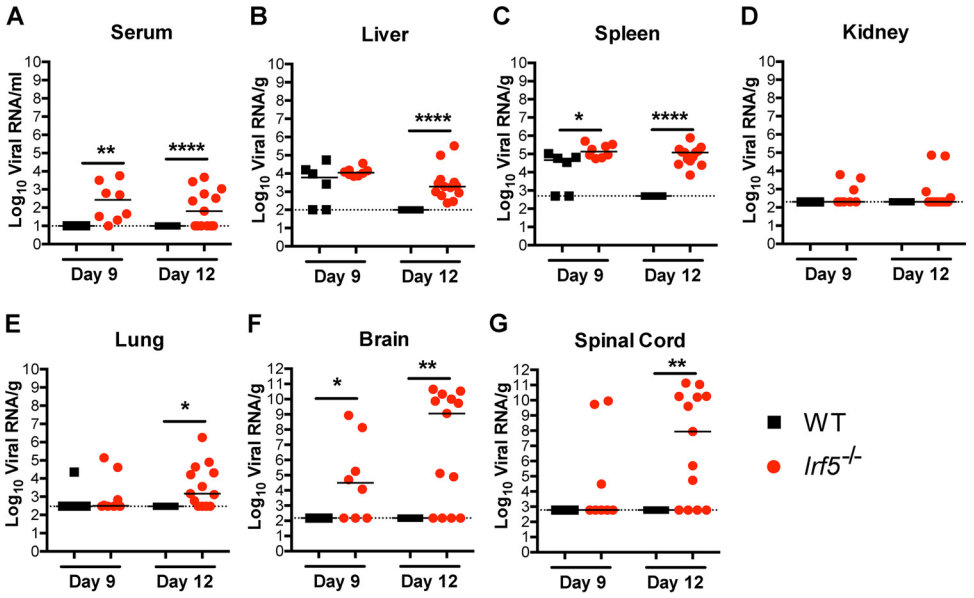

FIG 8 OROV RNA is detected in *Irf5*$^{-/-}$ mice at later time points. The viral burden after OROV infection of WT and *Irf5*$^{-/-}$ mice was determined by qRT-PCR in samples from serum (A), liver (B), spleen (C), kidney (D), lung (E), brain (F), and spinal cord (G). Data points represent individual mice. Bars indicate median values and were obtained from 6 to 13 mice per time point. Dashed lines represent the limit of sensitivity of the assay. Asterisks indicate statistical significance as judged by the Mann-Whitney test (*, $P < 0.05$; **, $P < 0.01$; ****, $P < 0.0001$).

adoptively transferred WT + μMT (lacking all mature B cells) or *Irf5*$^{-/-}$ + μMT bone marrow cells from CD45.2 mice into sublethally irradiated 4-week-old WT CD45.1 recipient mice. Eight weeks later, the reconstitution of donor immune cell populations in blood was confirmed by flow cytometry and all recipient animals were infected with 10^6 FFU of OROV (data not shown). However, no difference in weight loss or viral load in the brain at day 12 was observed between the two groups (data not shown). Thus, we did not observe a B cell-intrinsic role for IRF-5 in protection against OROV infection in the CNS.

IRF-5 restricts the neuropathogenesis of other orthobunyavirus. To evaluate whether IRF-5 also restricts infection of other orthobunyaviruses *in vivo*, we infected 8-week-old WT, *Irf5*$^{-/-}$, *Irf3*$^{-/-}$ *Irf7*$^{-/-}$ DKO, and *Irf3*$^{-/-}$ *Irf5*$^{-/-}$ *Irf7*$^{-/-}$ TKO mice with LACV (10^5 FFU), a related encephalitic orthobunyavirus. Similar to our results with OROV, rapid lethality was observed after LACV infection of *Irf3*$^{-/-}$ *Irf7*$^{-/-}$ DKO and *Irf3*$^{-/-}$ *Irf5*$^{-/-}$ *Irf7*$^{-/-}$ TKO mice (Fig. 12A). Remarkably, *Irf5*$^{-/-}$ mice infected with LACV failed to gain weight, showed clinical signs of neuroinvasive disease, and succumbed to infection after day 9 (Fig. 12B to E). Consistent with this, higher titers of LACV were observed in the brains and spinal cords (290- to 50,000-fold, $P < 0.05$) of *Irf5*$^{-/-}$ mice at days 8 and 12 after infection than in those of WT mice (Fig. 12F and G). These results establish that IRF-5 restricts infection and neuropathogenesis of two different orthobunyaviruses.

DISCUSSION

Our study describes an innate immune mechanism for restricting neuroinvasion of two different orthobunyaviruses that cause meningitis and encephalitis. IRF-5, a transcription factor that is activated after recognition of pathogen-associated molecular patterns (4), orchestrates a host response that controls bunyavirus neuroinvasion in infected mice. *Irf5*$^{-/-}$ mice died beginning at 12 days after OROV infection, a time when high levels of infectious virus were detected exclusively in the brain and spinal cord. The relative importance of IRF-5 to the antiviral response against OROV is highlighted by comparisons with *Irf3*$^{-/-}$ or *Irf7*$^{-/-}$ single-KO mice, which sustained no or substantially lower levels of mortality after infection (25). Moreover, significant levels of OROV infection were observed in the CNS of *Irf5*$^{-/-}$ but not *Irf3*$^{-/-}$ *Irf7*$^{-/-}$ DKO mice. Thus, IRF-5, rather than IRF-3 and/or IRF-7, regulates a stage in the control of OROV pathogenesis that prevents dissemination to the brain and spinal cord.

Apart from its effect on neuroinvasion, IRF-5 also restricted OROV replication in the liver, spleen, and blood at earlier stages of infection. The evidence for this comes from studies with *Irf5*$^{-/-}$ mice and also by comparing OROV pathogenesis between *Irf3*$^{-/-}$ *Irf7*$^{-/-}$ DKO and *Irf3*$^{-/-}$ *Irf5*$^{-/-}$ *Irf7*$^{-/-}$ TKO mice. The *Irf3*$^{-/-}$ *Irf5*$^{-/-}$ *Irf7*$^{-/-}$ TKO mice were highly vulnerable to OROV infection and succumbed with kinetics similar to those for *Ifnar*$^{-/-}$ mice (25), whereas DKO mice were less susceptible. Accordingly, the levels of infectious virus in the liver, spleen, and blood were higher in *Irf3*$^{-/-}$ *Irf5*$^{-/-}$ *Irf7*$^{-/-}$ TKO mice than n *Irf3*$^{-/-}$ *Irf7*$^{-/-}$ DKO mice (25). Consistent with a role for IRF-5 in restricting OROV replication in peripheral organs, higher levels of viral RNA were detected in the serum, liver, spleen, and kidneys of *Irf5*$^{-/-}$ than in WT mice at day 6 after infection.

OROV infection of 5- to 6-week-old *Irf5*$^{-/-}$ mice caused encephalitis after subcutaneous inoculation. The morphology of the antigen-positive cells observed in the brains of *Irf5*$^{-/-}$ mice was consistent with neurons as a primary target of infection. Previously, OROV was reported to cause encephalitis in newborn inbred WT mice and was associated with paralysis and mortality (31). OROV was recovered from the brain and spinal cord at days 4 and 5 after infection of newborns and was detected almost exclusively in neurons (31). OROV also induced meningoencephalitis in adult golden hamsters, with viral antigen present in brain cells that morphologically resembled neurons (35). We also ob-

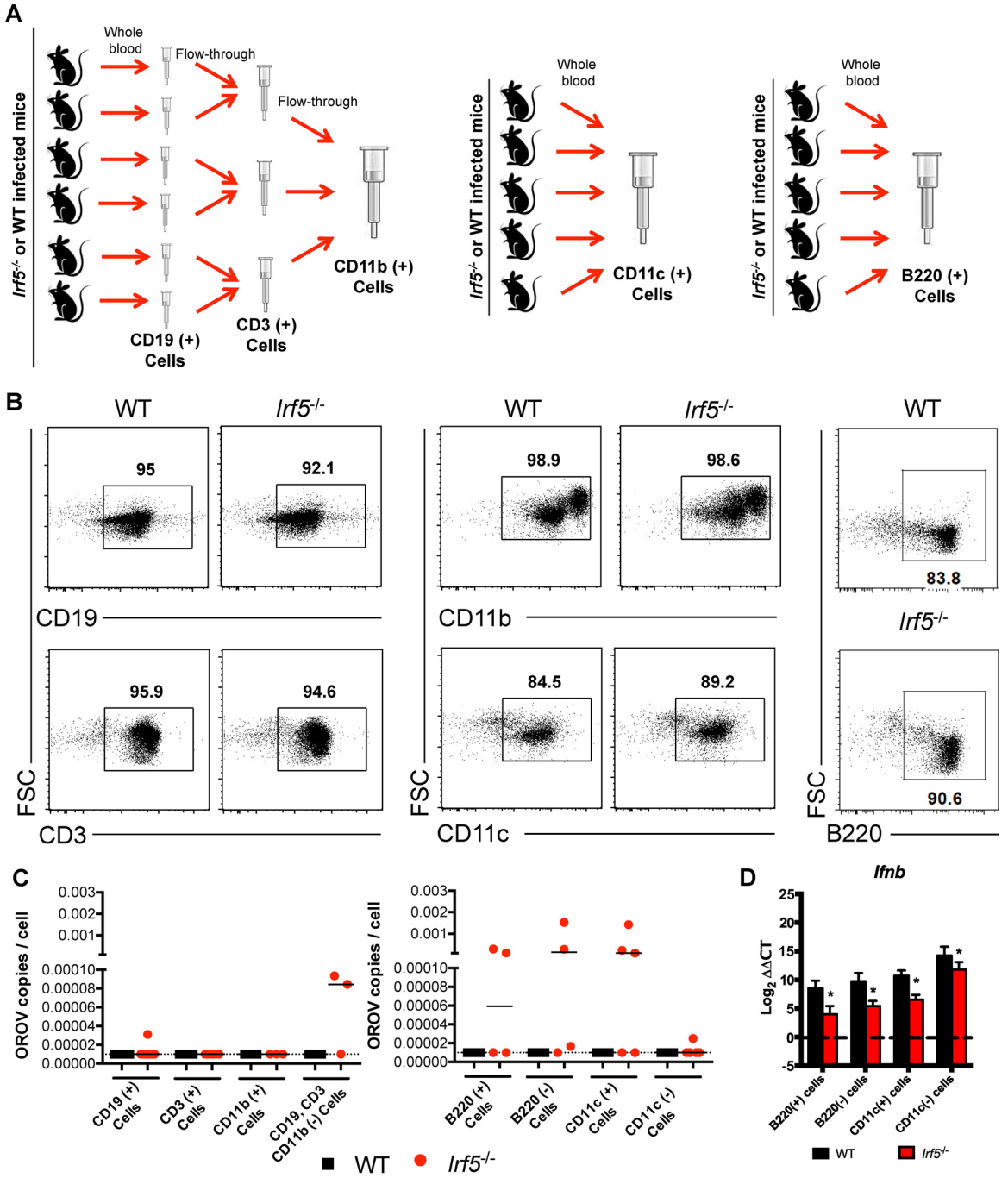

FIG 9 OROV induces less type I IFN production in circulating DC populations from *Irf5*$^{-/-}$ mice at late time points after OROV infection. (A) Cell isolation scheme. CD3, CD19^{+}, CD11b^{+}, CD11c^{+}, and B220^{+} cells were purified at day 8 after OROV infection from WT and *Irf5*$^{-/-}$ mice by positive selection using antibody-coated magnetic beads. CD19^{+} cells were purified from the whole blood of 6 WT and *Irf5*$^{-/-}$ mice, and the CD3^{+} and CD11b^{+} cells were sequentially purified using the flowthrough from CD19^{+} and CD3^{+} cells, respectively. As CD19-, CD3-, and CD11b-negative cells had detectable OROV RNA only in *Irf5*$^{-/-}$ mice, CD11c^{+} cells and B220^{+} cells subsequently were purified directly from whole blood pooled of 5 WT and *Irf5*$^{-/-}$ mice. (B) Flow cytometry of the different cell populations purified by positive selection, showing the forward scatter (FSC) versus staining with the specific antibody conjugated with fluorescein isothiocyanate (FITC). The percentage of specific positive cells is shown in the gate. (C) Number of copies of OROV RNA per cell in the different cells populations as determined by qRT-PCR after normalization to *Gapdh*. Each symbol indicates results from pools of mice, following the scheme described above. (D) Relative expression levels of *Ifnb* mRNA as determined by qRT-PCR. Gene expression was normalized to *Gapdh* mRNA and is shown as the fold increase compared to the cells from mock-infected mice on a $\log_2$ scale. The basal level of *Ifnb* mRNA was barely detectable and was similar in cells from WT and *Irf5*$^{-/-}$ mice. Data represent the averages from three independent experiments performed in triplicate and are expressed as the means ± SD, and asterisks indicate statistical significance (*, $P < 0.05$) as determined by 2-way ANOVA. The dotted line represents the limit of detection.

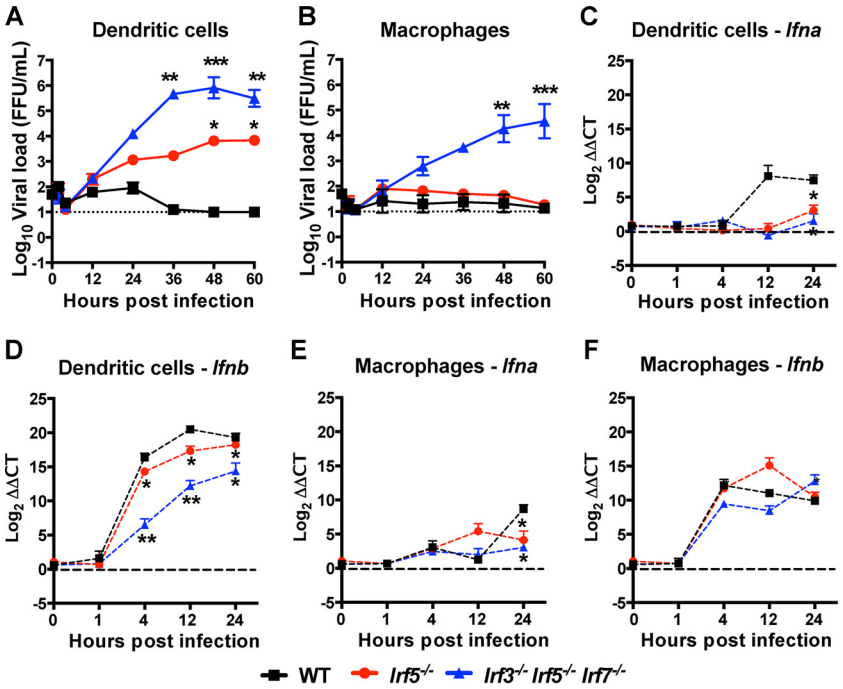

FIG 10 OROV replicates in cultured DCs but not Mϕ from *Irf5*$^{-/-}$ mice. (A and B) Kinetics of OROV replication in bone marrow-derived DCs (A) and Mϕ (B) from WT, *Irf5*$^{-/-}$, and *Irf3*$^{-/-}$ *Irf5*$^{-/-}$ *Irf7*$^{-/-}$ TKO mice after infection at an MOI of 0.001. The data represent the mean ± SD of three independent experiments performed in triplicate. All KO cell groups were compared to the WT by a two-way ANOVA, and asterisks indicate statistical significance (*, $P < 0.05$; **, $P < 0.01$; ***, $P < 0.001$). The dotted line represents the limit of detection of the assay. (C to F) Kinetics of *Ifna* (C and E) and *Ifnb* (D and F) expression in bone marrow-derived DCs (C and D) and Mϕ (E and F) from WT, *Irf5*$^{-/-}$, and *Irf3*$^{-/-}$ *Irf5*$^{-/-}$ *Irf7*$^{-/-}$ TKO mice after infection with OROV using an MOI of 0.001. The relative levels of *Ifna* and *Ifnb* mRNAs were determined by qRT-PCR after normalization to *Gapdh* mRNA and are displayed as $\Delta\Delta C_T$ values compared to the mock-infected cells on a $\log_2$ scale. The basal levels of *Ifna* and *Ifnb* mRNAs were barely detectable and were similar in cells from WT and *Irf5*$^{-/-}$ mice. Data represent the averages from three independent experiments performed in triplicate and are expressed as the means ± SD. The asterisks indicate statistical significance by two-way ANOVA (*, $P < 0.05$; **, $P < 0.01$), and the dotted line represents the limit of detection.

served that ~40% of 8-week-old *Irf5*$^{-/-}$ mice infected with LACV developed signs of neurological involvement, including dyskinesia and paresis. In all symptomatic animals, we recovered infectious LACV.

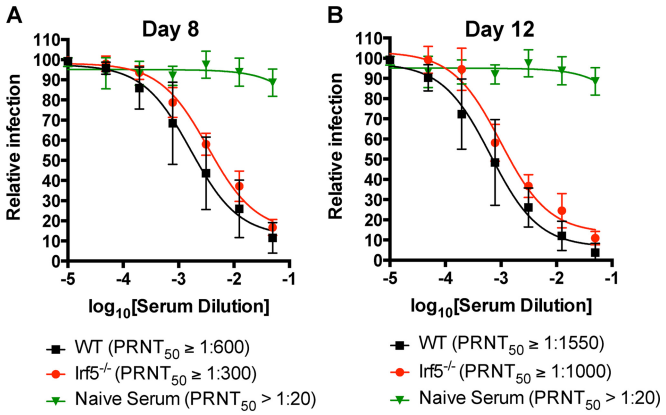

FIG 11 Effect of IRF-5 on the early antibody response in OROV-infected mice. The presence of neutralizing antibody in the sera from WT and *Irf5*$^{-/-}$ mice at 8 (A) and 12 (B) days after OROV infection as judged by a plaque reduction assay in Vero cells after incubation with 100 PFU of OROV and $\log_2$ dilutions of the tested serum is shown. Data represent the means for 8 mice per group from two independent experiments performed in duplicate. All error bars represent the SD. The $PRNT_{50}$ represents the dilution that showed 50% reduction in plaque formation in comparison with a control without serum after linear regression analysis.

How does IRF-5 control bunyavirus neuropathogenesis? We initially hypothesized that IRF-5 could affect viral replication directly in neurons. However, and as seen with the unrelated encephalitic flavivirus WNV (11), no major differences in viral burden in the brain were observed between WT and *Irf5*$^{-/-}$ mice after intracranial inoculation of OROV. This result suggests that the protective effect of IRF-5 against OROV or LACV is not due to a CNS-intrinsic antiviral mechanism. Given these findings, we evaluated whether a deficiency of IRF-5 affected OROV replication in circulating PBMCs, which could contribute to viremia or possibly crossing of virus into the brain via a "Trojan horse" mechanism (36). Analysis of viral RNA levels obtained from purified PBMC subsets of OROV-infected mice revealed that B220$^+$ and CD11c$^+$ cell subsets from *Irf5*$^{-/-}$ mice supported higher levels of OROV infection. However, these OROV-expressing cells were not sufficient to infect the CNS, as adoptive transfer of PBMCs or DCs from OROV-infected *Irf5*$^{-/-}$ mice did not induce disease in naive WT or *Irf5*$^{-/-}$ mice (data not shown). This result was not entirely unexpected, since infection of leukocytes alone does not disrupt the BBB in other viral models (37, 38). Although further experiments are warranted, IRF-5 could regulate expression of molecules that sustain the BBB integrity. An absence of IRF-5 then would result in increased viremia, infection of PBMCs, and BBB permeability, all of which together could promote virus neuroinvasion.

Because both B220$^+$ and CD11c$^+$ purified cells were positive

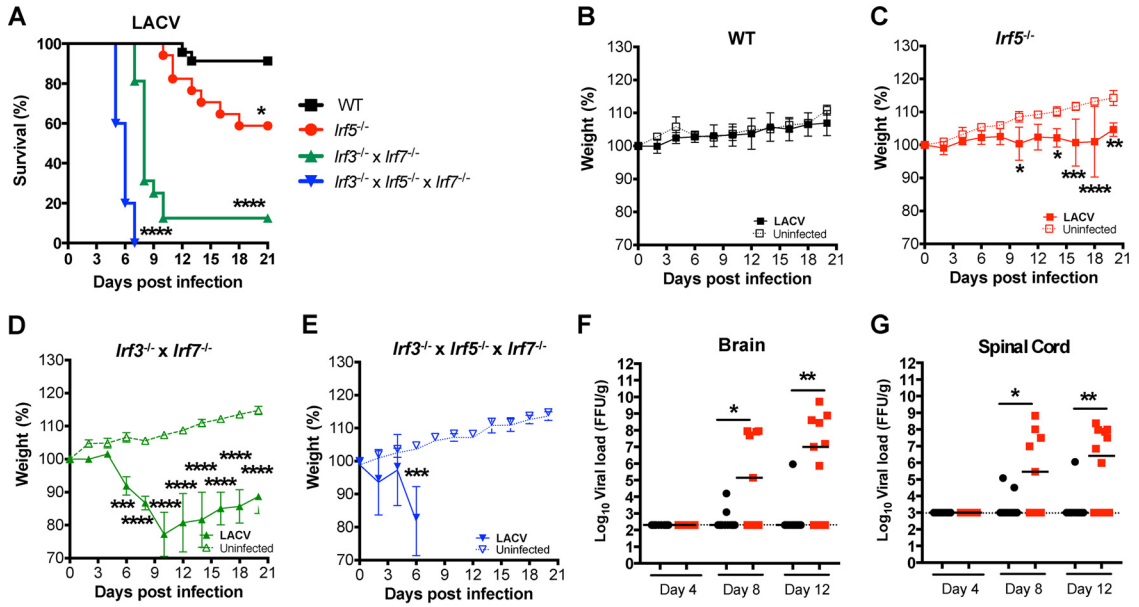

FIG 12 IRF-5 controls the neuropathogenesis of infection by LACV, a related orthobunyavirus. (A) Survival analysis of 8-week-old mice after inoculation with 10^5 FFU ($n = 23$ for WT, $n = 17$ for $Irf5^{-/-}$, $n = 16$ for $Irf3^{-/-}$ $Irf7^{-/-}$ DKO, and $n = 5$ for $Irf3^{-/-}$ $Irf5^{-/-}$ $Irf7^{-/-}$ TKO). Asterisks indicate differences that were statistically significant with a comparison to WT mice by the log rank test (*, $P < 0.05$; ****, $P < 0.0001$). (B to D) Weight loss analysis of 8-week-old mice after inoculation with 10^5 FFU of LACV by footpad inoculation in the same mice. Data are pooled from at least two independent experiments. Weight loss was compared by 2-way ANOVA. Asterisks indicate differences that were statistically significant with a comparison to WT animals with the same viral dose (*, $P < 0.05$; **, $P < 0.01$; ***, $P < 0.001$; ****, $P < 0.0001$). (F and G) The viral burden after LACV infection of WT or $Irf5^{-/-}$ mice was determined by qRT-PCR in samples from brain (F) and spinal cord (G). Data points represent individual mice. Bars indicate median values and were obtained from 8 to 12 mice per time point. Dashed lines represent the limit of sensitivity of the assay. Asterisks indicate statistical significance as judged by the Mann-Whitney test (*, $P < 0.05$; **, $P < 0.01$).

for OROV RNA at later time points (day 8) after viral infection, we speculated that the plasmacytoid DC (pDC) subset might be a primary target. IRF-5 regulates both IL-6 and IFN-β gene expression in pDCs (12), and these cells are a primary source of type I IFNs and proinflammatory cytokines after virus infection (17, 39). Although a definitive identification of pDCs as the key DC subset regulating CNS infection of OROV and LACV in $Irf5^{-/-}$ mice warrants further study, we observed lower expression levels of *Ifna* and *Ifnb* mRNAs after OROV infection in DCs *in vivo* and in cell culture. Thus, infection of specific subsets of DCs, including possibly pDCs, could modulate the production of antiviral cytokines and control of viral infection in blood. For bunyaviruses, this process appears to require an optimal IRF-5 signaling pathway, as in its absence viral persistence in serum occurs, and this is associated with neuroinvasion. This process appears to be cell type dependent, as in Mϕ an absence of IRF-5 did not impact OROV infection or IFN-β induction, and we observed no decrease in overall type I IFN levels in the sera of $Irf5^{-/-}$ mice at day 1, 2, or 3 after infection. Rather, type I IFN levels were higher in the sera of $Irf5^{-/-}$ mice at day 3 after infection; although the mechanism remains uncertain, this phenotype could reflect greater levels of OROV replication in another cell type or tissue.

IRF-5 is essential to B cell differentiation and modulates the expression of the plasma B cell maturation factor Blimp-1 (9). $Irf5^{-/-}$ mice have fewer T cells, B cells, NK cells, Mϕ, and DCs in the draining lymph nodes at day 2 after WNV infection than WT mice, and these mice have defects in generating an optimal acute and memory B cell response (11). Although $Irf5^{-/-}$ mice had slightly lower levels of neutralizing antibody against OROV at day 7 after infection, it is unclear if these small differences contributed to neuroinvasion. Bone marrow chimera reconstitution studies failed to show a protective role for IRF-5 in the B cell compartment.

In summary, our study shows that IRF-5 is a key component of the immune response against orthobunyaviruses and contributes to restricting neuroinvasion. This phenotype was associated with the defects in the control of replication and clearance of virus from circulating PBMCs. The persistent circulation of virus in the blood of $Irf5^{-/-}$ mice correlated with neuroinvasion and viral burden in the brain and spinal cord. Future studies with conditionally targeted IRF-5-deficent mice are planned to define the role of IRF-5 in specific cell types on neuroinvasion. The animal model described here may be useful for understanding the basic biology of the encephalitis induced by OROV, as well as for testing candidate therapeutics and vaccines. Finally, the antiviral activity of IRF-5 against different families of viruses capable of causing lethal CNS infection could explain the selection and perpetuation of gain-of-function *IRF5* alleles in the human population.

ACKNOWLEDGMENTS

This work was supported by the National Institutes of Health (R01 AI104972 and U19 AI083019 to M.S.D and P30 DK52574 to the Digestive Diseases Research Core Center Morphology Core), Conselho Nacional de Desenvolvimento Científico e Tecnológico (CNPq)—Science Without Borders (246513/2012-8 to J.L.P.-M), and a University Research Committee Award.

We gratefully acknowledge the technical assistance of Jennifer Govero, Michelle Noll, and Soila Sukupolvi-Petty.

FUNDING INFORMATION

HHS | NIH | National Institute of Allergy and Infectious Diseases (NIAID) provided funding to Michael S Diamond under grant numbers R01 AI104972 and U19 AI083019.

REFERENCES

1. **Taniguchi T, Ogasawara K, Takaoka A, Tanaka N.** 2001. IRF family of transcription factors as regulators of host defense. Annu Rev Immunol **19:**623–655. http://dx.doi.org/10.1146/annurev.immunol.19.1.623.
2. **Paun A, Pitha PM.** 2007. The IRF family, revisited. Biochimie **89:**744–753. http://dx.doi.org/10.1016/j.biochi.2007.01.014.
3. **Akira S, Uematsu S, Takeuchi O.** 2006. Pathogen recognition and innate immunity. Cell **124:**783–801. http://dx.doi.org/10.1016/j.cell.2006.02.015.
4. **Takaoka A, Yanai H, Kondo S, Duncan G, Negishi H, Mizutani T, Kano S, Honda K, Ohba Y, Mak TW, Taniguchi T.** 2005. Integral role of IRF-5 in the gene induction programme activated by Toll-like receptors. Nature **434:**243–249. http://dx.doi.org/10.1038/nature03308.
5. **Izaguirre A, Barnes BJ, Amrute S, Yeow WS, Megjugorac N, Dai J, Feng D, Chung E, Pitha PM, Fitzgerald-Bocarsly P.** 2003. Comparative analysis of IRF and IFN-alpha expression in human plasmacytoid and monocyte-derived dendritic cells. J Leukoc Biol **74:**1125–1138. http://dx.doi.org/10.1189/jlb.0603255.
6. **Barnes BJ, Richards J, Mancl M, Hanash S, Beretta L, Pitha PM.** 2004. Global and distinct targets of IRF-5 and IRF-7 during innate response to viral infection. J Biol Chem **279:**45194–45207. http://dx.doi.org/10.1074/jbc.M400726200.
7. **Mori T, Anazawa Y, Iiizumi M, Fukuda S, Nakamura Y, Arakawa H.** 2002. Identification of the interferon regulatory factor 5 gene (IRF-5) as a direct target for p53. Oncogene **21:**2914–2918. http://dx.doi.org/10.1038/sj.onc.1205459.
8. **Barnes BJ, Kellum MJ, Pinder KE, Frisancho JA, Pitha PM.** 2003. Interferon regulatory factor 5, a novel mediator of cell cycle arrest and cell death. Cancer Res **63:**6424–6431.
9. **Lien C, Fang CM, Huso D, Livak F, Lu R, Pitha PM.** 2010. Critical role of IRF-5 in regulation of B-cell differentiation. Proc Natl Acad Sci U S A **107:**4664–4668. http://dx.doi.org/10.1073/pnas.0911193107.
10. **Panchanathan R, Liu H, Liu H, Fang CM, Erickson LD, Pitha PM, Choubey D.** 2012. Distinct regulation of murine lupus susceptibility genes by the IRF5/Blimp-1 axis. J Immunol **188:**270–278. http://dx.doi.org/10.4049/jimmunol.1102311.
11. **Thackray LB, Shrestha B, Richner JM, Miner JJ, Pinto AK, Lazear HM, Gale M, Jr, Diamond MS.** 2014. Interferon regulatory factor 5-dependent immune responses in the draining lymph node protect against West Nile virus infection. J Virol **88:**11007–11021. http://dx.doi.org/10.1128/JVI.01545-14.
12. **Steinhagen F, McFarland AP, Rodriguez LG, Tewary P, Jarret A, Savan R, Klinman DM.** 2013. IRF-5 and NF-kappaB p50 co-regulate IFN-beta and IL-6 expression in TLR9-stimulated human plasmacytoid dendritic cells. Eur J Immunol **43:**1896–1906. http://dx.doi.org/10.1002/eji.201242792.
13. **Graham RR, Kozyrev SV, Baechler EC, Reddy MV, Plenge RM, Bauer JW, Ortmann WA, Koeuth T, Gonzalez Escribano MF, Argentine Spanish Collaborative G, Pons-Estel B, Petri M, Daly M, Gregersen PK, Martin J, Altshuler D, Behrens TW, Alarcon-Riquelme ME.** 2006. A common haplotype of interferon regulatory factor 5 (IRF5) regulates splicing and expression and is associated with increased risk of systemic lupus erythematosus. Nat Genet **38:**550–555. http://dx.doi.org/10.1038/ng1782.
14. **Miceli-Richard C, Comets E, Loiseau P, Puechal X, Hachulla E, Mariette X.** 2007. Association of an IRF5 gene functional polymorphism with Sjogren's syndrome. Arthritis Rheumatism **56:**3989–3994. http://dx.doi.org/10.1002/art.23142.
15. **Kristjansdottir G, Sandling JK, Bonetti A, Roos IM, Milani L, Wang C, Gustafsdottir SM, Sigurdsson S, Lundmark A, Tienari PJ, Koivisto K, Elovaara I, Pirttila T, Reunanen M, Peltonen L, Saarela J, Hillert J, Olsson T, Landegren U, Alcina A, Fernandez O, Leyva L, Guerrero M, Lucas M, Izquierdo G, Matesanz F, Syvanen AC.** 2008. Interferon regulatory factor 5 (IRF5) gene variants are associated with multiple sclerosis in three distinct populations. J Med Genet **45:**362–369. http://dx.doi.org/10.1136/jmg.2007.055012.
16. **Dideberg V, Kristjansdottir G, Milani L, Libioulle C, Sigurdsson S, Louis E, Wiman AC, Vermeire S, Rutgeerts P, Belaiche J, Franchimont D, Van Gossum A, Bours V, Syvanen AC.** 2007. An insertion-deletion polymorphism in the interferon regulatory factor 5 (IRF5) gene confers risk of inflammatory bowel diseases. Hum Mol Genet **16:**3008–3016. http://dx.doi.org/10.1093/hmg/ddm259.
17. **Paun A, Reinert JT, Jiang Z, Medin C, Balkhi MY, Fitzgerald KA, Pitha PM.** 2008. Functional characterization of murine interferon regulatory factor 5 (IRF-5) and its role in the innate antiviral response. J Biol Chem **283:**14295–14308. http://dx.doi.org/10.1074/jbc.M800501200.
18. **Lazear HM, Lancaster A, Wilkins C, Suthar MS, Huang A, Vick SC, Clepper L, Thackray L, Brassil MM, Virgin HW, Nikolich-Zugich J, Moses AV, Gale M, Jr, Fruh K, Diamond MS.** 2013. IRF-3, IRF-5, and IRF-7 coordinately regulate the type I IFN response in myeloid dendritic cells downstream of MAVS signaling. PLoS Pathog **9:**e1003118. http://dx.doi.org/10.1371/journal.ppat.1003118.
19. **Vasconcelos HB, Nunes MR, Casseb LM, Carvalho VL, Pinto da Silva EV, Silva M, Casseb SM, Vasconcelos PF.** 2011. Molecular epidemiology of Oropouche virus, Brazil. Emerg Infect Dis **17:**800–806. http://dx.doi.org/10.3201/eid1705.101333.
20. **Forshey BM, Guevara C, Laguna-Torres VA, Cespedes M, Vargas J, Gianella A, Vallejo E, Madrid C, Aguayo N, Gotuzzo E, Suarez V, Morales AM, Beingolea L, Reyes N, Perez J, Negrete M, Rocha C, Morrison AC, Russell KL, Blair PJ, Olson JG, Kochel TJ, NMRCD Febrile Surveillance Working Group.** 2010. Arboviral etiologies of acute febrile illnesses in Western South America, 2000-2007. PLoS Negl Trop Dis **4:**e787. http://dx.doi.org/10.1371/journal.pntd.0000787.
21. **Watts DM, Lavera V, Callahan J, Rossi C, Oberste MS, Roehrig JT, Cropp CB, Karabatsos N, Smith JF, Gubler DJ, Wooster MT, Nelson WM, Hayes CG.** 1997. Venezuelan equine encephalitis and Oropouche virus infections among Peruvian army troops in the Amazon region of Peru. Am J Trop Med Hyg **56:**661–667.
22. **Bastos Mde S, Figueiredo LT, Naveca FG, Monte RL, Lessa N, Pinto de Figueiredo RM, Gimaque JB, Pivoto Joao G, Ramasawmy R, Mourao MP.** 2012. Identification of Oropouche orthobunyavirus in the cerebrospinal fluid of three patients in the Amazonas, Brazil. Am J Trop Med Hyg **86:**732–735. http://dx.doi.org/10.4269/ajtmh.2012.11-0485.
23. **Bastos MS, Lessa N, Naveca FG, Monte RL, Braga WS, Figueiredo LT, Ramasawmy R, Mourao MP.** 2014. Detection of herpesvirus, enterovirus, and arbovirus infection in patients with suspected central nervous system viral infection in the Western Brazilian Amazon. J Med Virol **86:**1522–1527. http://dx.doi.org/10.1002/jmv.23953.
24. **Pinheiro FP, Rocha AG, Freitas RB, Ohana BA, Travassos da Rosa AP, Rogerio JS, Linhares AC.** 1982. Meningitis associated with Oropouche virus infections. Rev Instit Med Trop Sao Paulo **24:**246–251.
25. **Proenca-Modena JL, Sesti-Costa R, Pinto AK, Richner JM, Lazear HM, Lucas T, Hyde JL, Diamond MS.** 2015. Oropouche virus infection and pathogenesis is restricted by MAVS, IRF-3, IRF-7, and type I IFN signaling pathways in nonmyeloid cells. J Virol **89:**4720–4737. http://dx.doi.org/10.1128/JVI.00077-15.
26. **Daffis S, Suthar MS, Szretter KJ, Gale M, Jr, Diamond MS.** 2009. Induction of IFN-beta and the innate antiviral response in myeloid cells occurs through an IPS-1-dependent signal that does not require IRF-3 and IRF-7. PLoS Pathog **5:**e1000607. http://dx.doi.org/10.1371/journal.ppat.1000607.
27. **Takaoka A, Mitani Y, Suemori H, Sato M, Yokochi T, Noguchi S, Tanaka N, Taniguchi T.** 2000. Cross talk between interferon-gamma and -alpha/beta signaling components in caveolar membrane domains. Science **288:**2357–2360. http://dx.doi.org/10.1126/science.288.5475.2357.
28. **Thackray LB, Duan E, Lazear HM, Kambal A, Schreiber RD, Diamond MS, Virgin HW.** 2012. Critical role for interferon regulatory factor 3 (IRF-3) and IRF-7 in type I interferon-mediated control of murine norovirus replication. J Virol **86:**13515–13523. http://dx.doi.org/10.1128/JVI.01824-12.
29. **Livak KJ, Schmittgen TD.** 2001. Analysis of relative gene expression data using real-time quantitative PCR and the 2(−Delta Delta C(T)) method. Methods **25:**402–408. http://dx.doi.org/10.1006/meth.2001.1262.
30. **Diamond MS, Sitati EM, Friend LD, Higgs S, Shrestha B, Engle M.** 2003. A critical role for induced IgM in the protection against West Nile virus infection. J Exp Med **198:**1853–1862. http://dx.doi.org/10.1084/jem.20031223.
31. **Santos RI, Almeida MF, Paula FE, Rodrigues AH, Saranzo AM, Paula AE, Silva ML, Correa VM, Acrani GO, Neder L, Arruda E.** 2012. Experimental infection of suckling mice by subcutaneous inoculation

with Oropouche virus. Virus Res **170:**25–33. http://dx.doi.org/10.1016/j.virusres.2012.07.006.

32. **Ferenczy MW, Marshall LJ, Nelson CD, Atwood WJ, Nath A, Khalili K, Major EO.** 2012. Molecular biology, epidemiology, and pathogenesis of progressive multifocal leukoencephalopathy, the JC virus-induced demyelinating disease of the human brain. Clin Microbiol Rev **25:**471–506. http://dx.doi.org/10.1128/CMR.05031-11.
33. **Maginnis MS, Stroh LJ, Gee GV, O'Hara BA, Derdowski A, Stehle T, Atwood WJ.** 2013. Progressive multifocal leukoencephalopathy-associated mutations in the JC polyomavirus capsid disrupt lactoseries tetrasaccharide c binding. mBio **4:**e00247–13. http://dx.doi.org/10.1128/mBio.00247-13.
34. **Yasuda K, Nundel K, Watkins AA, Dhawan T, Bonegio RG, Ubellacker JM, Marshak-Rothstein A, Rifkin IR.** 2013. Phenotype and function of B cells and dendritic cells from interferon regulatory factor 5-deficient mice with and without a mutation in DOCK2. Int Immunol **25:**295–306. http://dx.doi.org/10.1093/intimm/dxs114.
35. **Rodrigues AH, Santos RI, Arisi GM, Bernardes ES, Silva ML, Rossi MA, Lopes MB, Arruda E.** 2011. Oropouche virus experimental infection in the golden hamster (Mesocrisetus auratus). Virus Res **155:**35–41. http://dx.doi.org/10.1016/j.virusres.2010.08.009.
36. **Gras G, Kaul M.** 2010. Molecular mechanisms of neuroinvasion by monocytes-macrophages in HIV-1 infection. Retrovirology **7:**30. http://dx.doi.org/10.1186/1742-4690-7-30.
37. **Roe K, Kumar M, Lum S, Orillo B, Nerurkar VR, Verma S.** 2012. West Nile virus-induced disruption of the blood-brain barrier in mice is characterized by the degradation of the junctional complex proteins and increase in multiple matrix metalloproteinases. J Gen Virol **93:**1193–1203. http://dx.doi.org/10.1099/vir.0.040899-0.
38. **Roe K, Orillo B, Verma S.** 2014. West Nile virus-induced cell adhesion molecules on human brain microvascular endothelial cells regulate leukocyte adhesion and modulate permeability of the in vitro blood-brain barrier model. PLoS One **9:**e102598. http://dx.doi.org/10.1371/journal.pone.0102598.
39. **Siegal FP, Kadowaki N, Shodell M, Fitzgerald-Bocarsly PA, Shah K, Ho S, Antonenko S, Liu YJ.** 1999. The nature of the principal type 1 interferon-producing cells in human blood. Science **284:**1835–1837. http://dx.doi.org/10.1126/science.284.5421.1835.